EVALUATION OF SPRINGBACK PREDICTION CAPABILITY USING UNIFORM PURE BENDING

A Thesis by

Kunal Indravadan Patel

Bachelor of Engineering, Sardar Patel University, India, 2002

Submitted to the College of Engineering
and the faculty of Graduate School of
Wichita State University
in partial fulfillment of
the requirements for the degree of
Master of Science

May 2006

EVALUATION OF SPRINGBACK PREDICTION CAPABILITY USING UNIFORM PURE BENDING

I have examined the final copy of this thesis for form and content and recommend that it be accepted in partial fulfillment of the requirements for the degree of Master of Science, with a major in Industrial and Manufacturing Engineering.

_____
Viswanathan Madhavan, Committee Chair

We have read this thesis
and recommend its acceptance:

_____
Don Malzahn, Committee Member

_____
Hamid Lankarani, Committee Member

DEDICATION

To HIM
and all I love

ACKNOWLEDGEMENTS

I would like to express my sincerest thanks and appreciation to my advisor Dr. Vis Madhavan. This would have been an impossible task without his untiring guidance and patient help throughout my thesis work. I am truly thankful to him for the time that he devoted to my work. He is among the few to directly or indirectly influence my thoughts and character.

I would also like to express hearty thanks to Dr. Hamid Lankarani and Dr. Don Malzahn for their time and effort in reviewing this work and suggesting constructive inputs.

I would like to thank Ms. Kristie Bixby for taking the time to review this manuscript. My friends Pranathi Aedla and Rajen Pandya helped me throughout my stay at Wichita State University, and I will be ever thankful to them. I would also like to acknowledge the help of all my friends who have directly or indirectly helped me throughout my graduate career.

ABSTRACT

The aim of this study is to develop uniform pure bending as an objective test for determining the accuracy of springback prediction by employing different FEA techniques. A complete theoretical solution for the bending moment and change in sheet thickness is available only for uniform pure bending of perfectly plastic sheets. However, plastic hinging develops naturally in simulations of bending perfectly plastic sheets. We have developed a method to prevent plastic hinging and achieve uniform pure bending of sheets by applying constraint equations to nodes along the center fiber. The error in the bending moment for forming (E_1), the error due to incomplete unloading during springback (E_2), and error in the change of curvature corresponding to the change in bending moment during unloading (E_3) are considered independently to get insights into the reasons for discrepancies between finite element analysis and theoretical results for springback.

Uniform pure bending is also used to study the bending moment and springback experienced with work-hardening materials. Comparisons have been made with analytical solutions containing minor approximations in terms of the behavior of the material near the center fiber, which is subject to reverse loading. The fact that two different theoretical models for the material undergoing reverse deformation yield results that differ by less than 1% leads to a high degree of confidence in the theoretical models. We have used uniform pure bending to study the inherent springback prediction capability of different types of element analysis, convergence parameters, and discretization level in two different finite element analysis packages, namely MARC and ABAQUS.

For simulations in ABAQUS using two dimensional elements and a perfectly plastic material model, the bending moment given by FEA is less than that predicted by the theoretical model by about -3%, indicating lesser springback than that predicted by theory. However for three dimensional elements, the bending moment is higher by about 10% for a relative curvature (χ) of 0.2. For a coarse discretization (about 4 elements around a 90° bend), this error increases to about 37%. For a work-hardening material model, two dimensional elements predict 12% less bending moment than the theory, indicating an under-prediction in springback. Shell elements with reduced integration give an under-prediction of springback and show a negative error value between 2% and 10% for the simulations with different integration points, while shell with full integration show a positive total error of abut 3%, indicating a higher springback than predicted by theory. Changing the convergence tolerance value by 100 from the default value shows a 2% change in calculated results. For MARC, the two dimensional elements under-predicts springback by 10%, while the three dimensional elements have shown over-prediction up to 30% in moment calculations.

Based on the findings, uniform pure bending is recommended as a benchmark test for identifying the intrinsic accuracy with which springback can be predicted by FEA simulations using different simulation parameters. Uniform pure bending can be used to develop effective guidelines for reliable finite element simulations of springback.

TABLE OF CONTENTS

LIST OF FIGURES

LIST OF TABLES

CHAPTER 1

INTRODUCTION

1.1. Need for An Objective Test for Springback Prediction Capability

Sheet metal forming is widely used in most industries for forming sheets into appropriate shapes by plastically deforming the sheet material beyond its yield strength to achieve permanent deformation. The design and manufacturing of the tools that accomplish this requires significant investment. Finite Element Analysis (FEA) is currently the most commonly used numerical method for analyzing metal forming (Paulsen et al., 1998). FEA based "virtual manufacturing" allows for a significant cost reduction in the development of the manufacturing process by substituting trial and error procedures with more effective numerical simulation techniques (Forcelesse et al., 1996). Numerous studies have validated the accuracy of FEA results with sheet metal forming data. Forcellese et al. (1996), studied V-punch and U-die bending by using explicit and implicit FEM codes. Zhou et al., (1996) studied convergence and CPU time requirements for predicting springback and wrinkling.

However, accurate calculation of springback, especially for cases involving large curvatures, is routinely still not feasible. According to Xu et al. (2004), analysis of the springback phase is complicated since it involves material and geometric non-linearity. It is therefore desirable to have a standard test that can help to provide guidance in developing accurate finite element simulations for predicting springback.

1.2. Sheet Metal Bending Processes in Industry

High–strength aluminum alloys are constantly being developed and adopted by the aircraft and automobile industries for increasing numbers of parts in order to satisfy higher strength–to–weight ratio requirements. Many of these parts are made by processes that involve

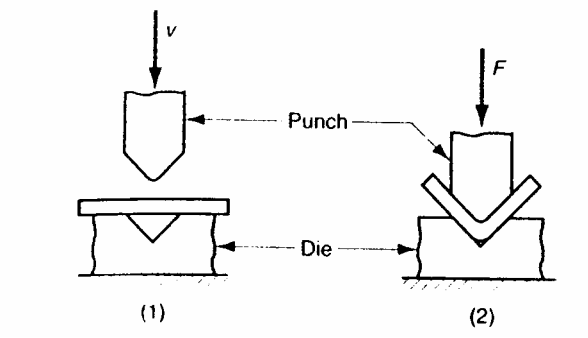

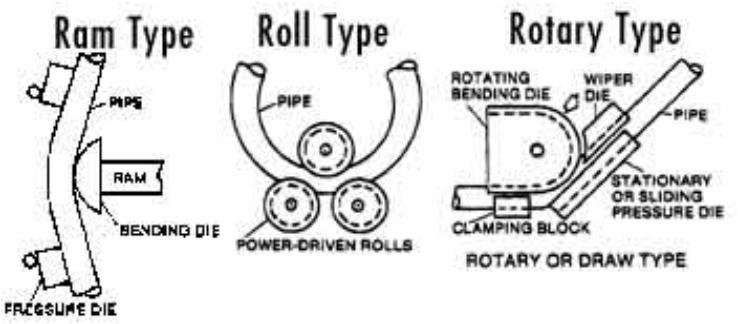

Figure 1. Different bending processes commonly used in industry (www.ttb.com/process.htm).

the bending of sheets. Sheet metal and pipe-forming processes that involve a significant amount of bending include v-bending, pipe/tube bending, and stretch bending. Figure 1 illustrates the kinematics of some of these processes. Developing the tools to carry out these processes usually requires estimating the springback of the part and compensating for the tool geometry, which ensures that the formed sheet after springback matches the required shape of the part. It is very important to predict springback quantitatively, as well as qualitatively, in order to reduce trial and error, rework and scrap.

Although bending is technically a simple process, it causes a complex history of induced stresses and movement of material in the blank. The processes illustrated in Figure 1 typically impose bending, stretching, and shear stresses on the blank. Friction, between the punch and the blank and between the blank and the die, plays a vital role in the deformation of the blank.

After bending is completed, the tool's action ceases. At this time, the bent sheet is not held by any constraining force and is free to relieve the internal elastic strains. This is seen as springback in the sheet. Predicting springback is complicated due to the complex stress and strain history the part undergoes during the bending process.

For most components, springback is compensated in the tooling that is used for bending. These tools are designed to bend the blank more than required so that the blank attains the desired shape after springback. The accuracy with which springback is compensated for determines the scrap rate of a process. Traditionally, empirical formulae and rules of thumb based on experimental trial-and-error have been used to design the processing route, profile geometry, and tooling. This is an expensive approach to the problem, warranting the use of numerical methods such as FEA to gain insights into the sheet forming and springback process (Paulsen et al., 1995). An accurate analysis of the elastic springback in bending is extremely important when determining the over-bending angle required to compensate for the springback effect (Forcellese et al., 1996).

Finite element analysis is increasingly being used to compensate springback in tools used for stampings, extrusions and stretched parts. The forming phase is increasingly simulated using the explicit time integration method (Maker, 1998) because it simplifies complex non-linear analyses by using contacts. Springback is almost always analyzed using an implicit time–integration scheme, which requires an iterative solver to converge with a solution within a specified convergence tolerance.

1.3. Objectives of this Study

The aim of this study is to develop an objective test that determines the accuracy of springback prediction when using different FEA techniques, element formulations, convergence

tolerances, and discretization levels that can also provide insights into causes for certain errors. Since only bending stresses are important in springback, uniform pure bending of sheet metal is a good candidate process to serve as an objective test for springback. *Pure bending* refers to the application of a pure moment at each section, with minimum membrane or shear stresses superimposed. *Uniform bending* refers to sheet bending processes where the curvature of the sheet remains constant for all the stages of forming so that end-effects arising from applied loads do not influence the results.

The advantage of uniform pure bending is that FEA solutions can be compared to available theoretical solutions for the bending moment and thickness as a function of bend radius, especially for a perfectly plastic material where an exact solution is available. Even for work-hardening materials, analytical solutions are available, with only minor approximations in terms of the behavior of material near the center fiber which is subject to reverse loading.

Choosing uniform pure bending for testing springback prediction capability, the objectives of this study are as follows: (i) developing a technique for achieving uniform pure bending in FEA simulations, (ii) analyzing the bending and springback stages independently and developing error estimates that provide insights into the accuracy of the simulation of each of the stages, and (iii) comparing the performance of different types of FEA, with different combinations of input parameters, to predict springback.

1.4 Organization of this Thesis

Chapter 2 highlights relevant studies in pure bending. Hill's theory (1950) for perfectly plastic material is discussed, as are work hardening material models proposed by Crafoord (1970) and Dadras and Majlessi (1982). Recent developments in the prediction of springback using FEA are also discussed.

Chapter 3 discusses the development of a methodology to simulate uniform pure bending of sheets by enforcing appropriate nodal constraints through user subroutines. By studying the error in bending moment prediction for the forming stage, the error due to incomplete unloading during the unloading stage, and the error in predicting the change of curvature corresponding to the change in the bending moment, insights regarding the sources of error and their relative magnitude is obtained.

In chapter 4, results obtained from two FEA packages (ABAQUS and MARC), are compared with theoretical results by Hill (1950), Crafoord (1970), and Dadras and Majlessi (1982). Guidelines to developing reliable finite element simulations for predicting springback are provided in chapter 5, based on observed error values for simulations with different element formulations, discretization level, loading type, and convergence tolerance values.

CHAPTER 2

LITERATURE REVIEW

Springback occurs when the tool forces are released from a formed sheet. Too much springback and poor dimensional accuracy causes parts to be scrapped. Accurate prediction and effective compensation of springback are difficult issues in sheet metal forming (Xu et al., 2004). Most plate sections deform under the action of a pure bending moment (Delannay et al., 2003). Johnson and Yu (1981) studied springback in beams, subjecting them to uniaxial and biaxial elastic-plastic pure bending. Leu (1995) used uniform pure bending to study the effect of anisotropy and strain hardening exponent on springback.

2.1. Stresses and Strains in Pure Bending

In a pure bending process, the sheet is bent solely by the application of a moment without any other external loads on the sheet. Pure bending is a theoretical concept and can only be approximated in practice. Figure 2 shows a sketch that includes the applied moments and the induced tangential and radial stresses in the sheet. Various parameters of interest in sheet bending are also indicated.

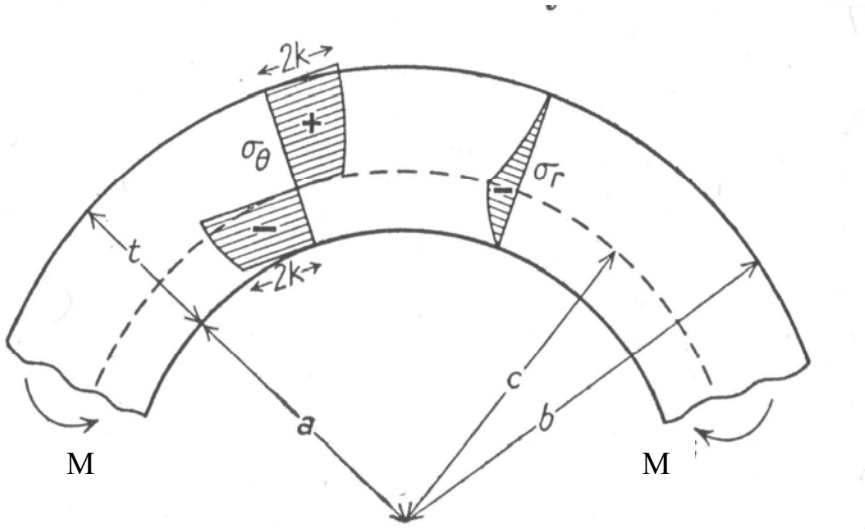

Figure 2. Analysis of pure bending (Hill, 1950).

For high curvatures, the compressive radial stresses (σ_{rr}) induced in the bend, due to the nature of stress equilibrium equations for curved beams, cannot be ignored. The circumferential stresses ($\sigma_{\theta\theta}$) are tensile along the top layer and compressive along the bottom layer. Since yielding of the sheet material depends on both $\sigma_{\theta\theta}$ and σ_{rr}, the compressive σ_{rr} causes the average $\sigma_{\theta\theta}$ in the layers subjected to compression to be higher in magnitude than the average $\sigma_{\theta\theta}$ in the layers subjected to tension. In order for the resultant membrane stress to be zero, the neutral axis is closer to the inner radius than to the outer radius ((b-c) > (c-a)).

While it is sufficient to divide the sheet into two zones, one in tension and the other in compression, for the analysis of bending of a perfectly plastic material, this is not the case for the bending of a work-hardening material. Following Wolter (1950) as described by Crafoord (1970), for work-hardening materials the bend needs to be divided into three zones through the thickness (shown schematically in Figure 3) based on the strains induced in the sheet.

i. Zone 1 consists of layers of material with a radius larger than that of the original central layer. The material in this region is subjected to monotonically increasing circumferential tension (elongation) during bending.

ii. Zone 2 consists of layers of material with a radius smaller than that of the neutral layer. The material in this region is subjected to monotonically increasing compression along the circumference.

iii. Zone 3 consists of layers of material that lie between the neutral layer and the original central layer. The material in this region is subjected initially to circumferential compression and later reverse-loaded in circumferential tension due to the migration of the neutral layer towards the inner radius. The reversal of stresses causes the material to show reduced yield stress which is a manifestation of the Bauschinger effect.

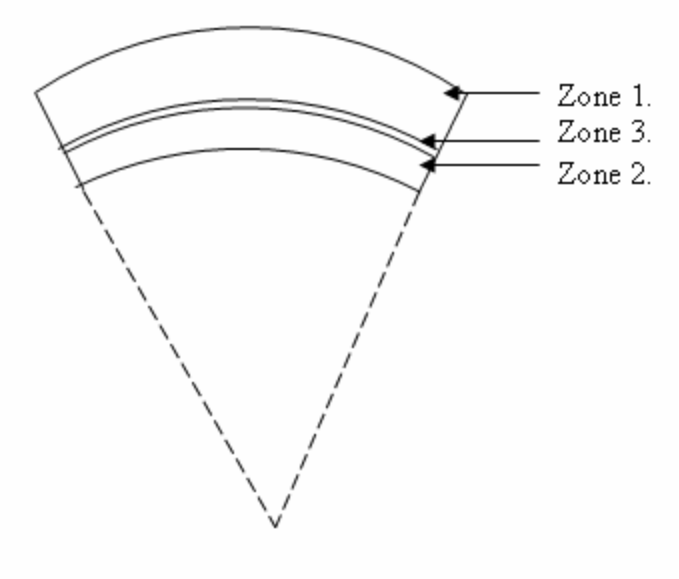

Figure 3. Different zones in a sheet bent to high curvature.

Figure 4 shows the deformation of the different layers as the sheet bends. The originally flat sheet (shown on the right) is divided into ten layers of equal thickness, with their boundaries marked from 0 to 10. According to elementary bending theory, interface 5 is the center fiber of the sheet and the neutral layer for bending. Layers above this interface are in tension, while layers below this are in compression. The bent configuration of the sheet shown in the left side of Figure 4 shows the thinning of the top layers and the thickening of the bottom layer by the time the sheet is bent to a relative curvature (χ=t/r_m) of approximately 1.0. The resulting difference between the radius of the center fiber of the sheet (r_c) and the mean radius of curvature ($r_m = (\frac{r_o + r_i}{2})$) can be easily perceived. As discussed above, due to the higher level of circumferential stresses in the bottom layer than the tensile stress in the top layer, the neutral layer lies below the mean layer as shown in Figure 4. Considering the fact that the layers above r_n are now in tension, and the layers below r_c were originally in compression, it can be deduced that Zone 3 extends from r_c to r_n.

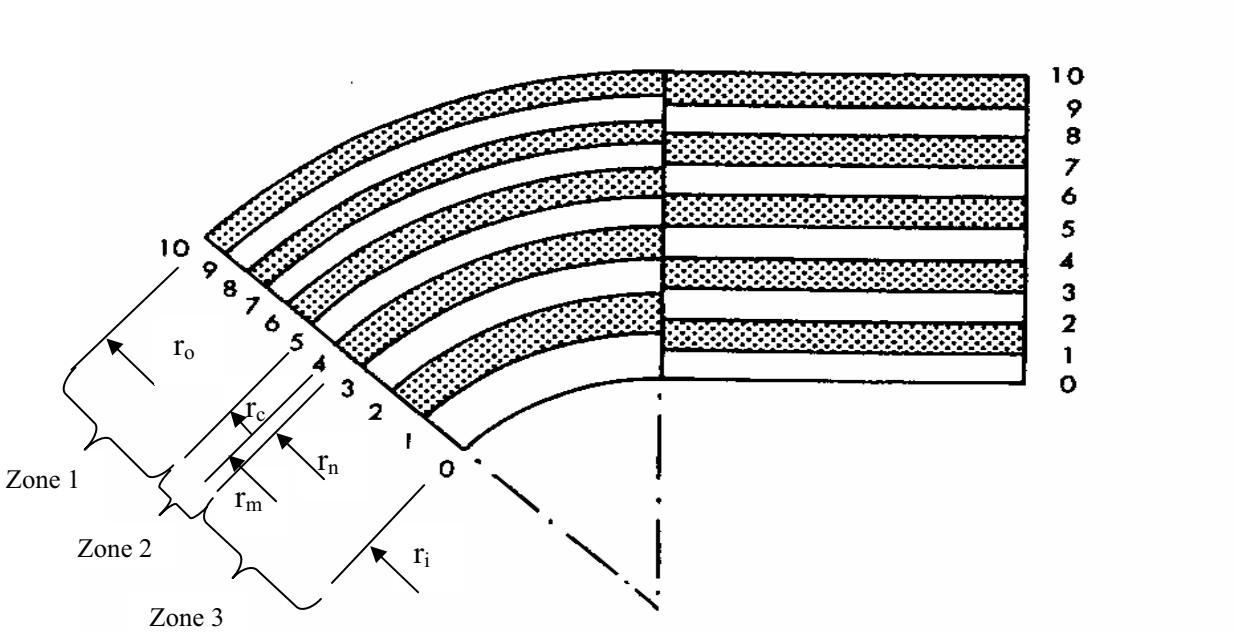

Figure 4. Movement of material in layers of the bent sheet (Wolter, 1950).

2.2. Theoretical Models for Pure Bending

Ludwik (1904) proposed a theory of pure bending. He assumed the neutral layer to coincide with the central layer of the sheet at different stages of bending. This theory ignores the radial stress distribution through the sheet thickness. The study provides a basis for further development of bending theory using perfectly plastic and work-hardening material models.

2.2.1. Hill's Theory

In 1950, Hill proposed a complete solution for pure bending of sheets for a perfectly plastic material model. The theory considers the radial stresses and the movement of layers in the sheet. It proves that the sheet thickness remains unchanged and the bending moment is constant throughout the bending operation. Hill's solution for a perfectly plastic material proposes a

constant moment of $\frac{2}{\sqrt{3}}\frac{Yt_0^2}{4}$ per unit width of the bend for all curvatures of the bend. It is predicted (without proof), that work-hardening causes thinning of the sheet.

2.2.2. Crafoord's Theory

Crafoord (1970) first developed an analysis of the bending of work-hardening materials, correctly satisfying the equilibrium equations, the boundary conditions and taking into account the change in thickness of the sheet. He used the stress-strain relations suggested by Voce (1948) (Equation 3 on page 19) to describe the strain hardening behavior of the material.

Crafoord's theory (1970) assumes that the yield strength of the material in the reverse bent region (Zone 3) is a constant value equal to the yield strength of the virgin material. Crafoord developed equations for the strains and stresses in the three zones in terms of the radial location, also taking into consideration the yield criterion (including radial stresses) and the boundary conditions. The relative sheet thickness ($\eta = t/t_0$), the relative radius of the neutral axis ($\rho=r_n/r_o$) and the bending moment ($M = \int \sigma_{\theta\theta}.rdr$) are obtained as functions of the relative curvature ($\chi=t/r_m$). The equation derived by Crafoord that relates the normalized bending moment (M/t^2) to the relative curvature (χ) is as follows:

$$\begin{aligned}\frac{M}{t^2} &= \left(\frac{1}{\chi}+0.5\right)^2\left[\frac{\alpha}{4}-\frac{\beta}{8}+\frac{\beta}{4}\ln\left(\frac{1+0.5\chi}{\eta}\right)+\frac{\gamma}{2\delta-4}\left(\frac{1+0.5\chi}{\eta}\right)^{-\delta}\right]+\\ &\left(\frac{1}{\chi}-0.5\right)^2\left[\frac{\alpha}{4}+\frac{\beta}{8}-\frac{\beta}{4}\ln\left(\frac{1-0.5\chi}{\eta}\right)-\frac{\gamma}{2\delta+4}\left(\frac{1-0.5\chi}{\eta}\right)^{\delta}\right]+\\ &\left(\frac{\eta}{\chi}\right)^2\left[\frac{\beta}{8}-\frac{\gamma}{4}+\frac{\gamma}{4-2\delta}\right]+\left(\frac{\rho\eta}{\chi}\right)^2\left[-\frac{\alpha}{2}-\frac{\beta}{8}+\frac{\beta}{4}+\frac{\gamma}{4}\ln\rho+\frac{\gamma}{4+2\delta}\rho^{\delta}\right]\end{aligned} \quad (1)$$

Where α, β, γ and δ are the parameters in the Voce material model. An explicit numerical calculation is employed to track ρ and η as a function of χ to calculate M. This is explained briefly in Appendix A.

Crafoord's work provides results for the dependence of M, η, and ρ on χ, for different material properties representing four different materials. Crafoord (1970) performed experiments that approximated uniform pure bending and obtained a close correlation between theoretical predictions and experimental results.

2.2.3. Dadras and Majlessi's Model

Dadras and Majlessi (1982) expanded Crafoord's work by introducing two different assumptions for the behavior of the fibers in Zone 3 subjected to reversed loading. The first model considers a linear stress-strain behavior for fibers in Zone 3 that are subject to reversed bending. The second model considers a kinematic hardening model using Ludwik's equation in order to simplify the stress equilibrium equations. Figure 5 (Dadras and Majlessi, 1982) shows the stress-strain histories of different points, A, B, D, E and F between r_c and r_n and clearly shows the different assumptions for the material strength in zone 3. The subscripts 0,1 and 2 indicate three bends of increasing curvature at which the strain and stresses are compared. For instance, the stress at point D at time 2 according to model 1 would be D_2, whereas the stress according to model 2 would be D_2'.

Dadras and Majlessi (1982) derived the following equation for the bending moment per unit width:

$$M = \frac{k_0}{2}(r_0^2 + r_i^2 - 2r_n^2) - \frac{k_2}{2}(r_o^2\varepsilon_0^{n+1} - r_i^2\varepsilon_i^{n+1}) + k_2 r_u^2 \left\{ \varepsilon_0^{n+1} \sum_{m=0}^{\alpha} \frac{\frac{2^m}{m!}(n+1+\frac{m}{2})}{n+m+1} \varepsilon_0^m - \varepsilon_i^{n+1} \sum_{m=0}^{\alpha} \frac{\frac{(-2)^m}{m!}(n+1+\frac{m}{2})}{n+m+1} \varepsilon_i^m \right\} \quad (2)$$

They adopted a procedure similar to that adopted by Crafoord for formulating the differential equations to derive the evolution of η, ρ and M with χ. They show plots of the radial stress and tangential stress for bending with different material properties. The radial stress is found to be compressive and continuous throughout the thickness. The tangential stress resembles the stress-strain curve of the material. Dadras and Majlessi also found that the bending moment initially increases with the deformation and then decreases as the bend progresses.

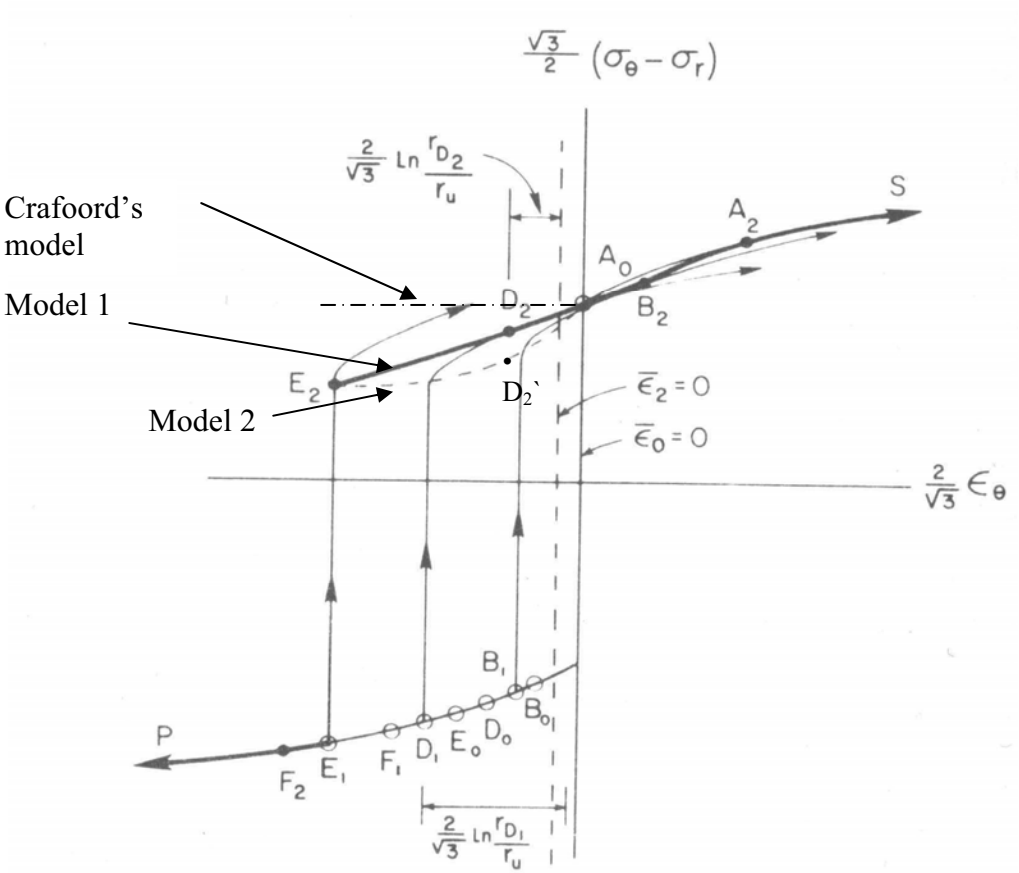

Figure 5. Schematic representation of stress-strain history for different fibers subjected to reverse loading.

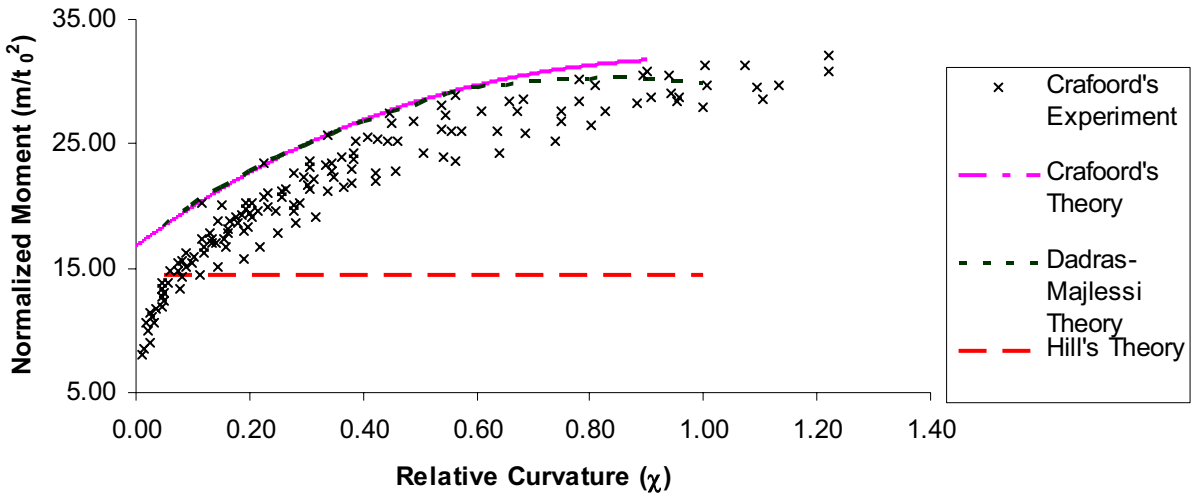

Figure 6. Comparison of theoretical models for the bending of perfectly plastic and work hardening materials with experimental results obtained by Crafoord (1970) (condition: aluminum, sheet thickness=4mm).

Figure 6 compares the bending moment predicted by Hill's, Crafoord's and Dadras and Majlessi's model for one condition. It also shows the experimental results obtained by Crafoord for the same condition.

2.3. Finite Element Analysis of Sheet Bending

Sheet metal bending can be simulated by finite element analysis using the implicit and explicit integration schemes. Implicit integration requires a force, or displacement–based convergence criterion, to be satisfied. In the forming stage, this leads to high analysis time. Therefore forming simulations for finite element analyses are typically done using the explicit time integration method. Explicit time integration is neither accurate nor efficient for the evaluation of elastic springback because, with the contact surfaces removed, the deformed sheet starts to oscillate around the new equilibrium position until the kinetic energy is totally dissipated (Micari et al., 1997). Springback is usually analyzed using the implicit time integration scheme, whereby accurate results can be obtained.

Bending deformation in numerical modeling has been approached in three ways: the membrane approach, the shell approach, and the 3-D (solid) element approach (Zhou et al., 1996). The selection of the number of integration points through the thickness for shell elements affects the accuracy of results. Xu et al. (2004) suggests a minimum of five integration points and recommends seven for reliable springback analysis. The increase in integration points comes with an increased CPU time requirement.

Mattiasson et al. (1995) proposed that the magnitude of springback is inversely proportional to the element size used in the FEA model. Stress relaxation is accurate for smaller element sizes such as 0.5 millimeters.

According to Cao et al. (1999), the most significant factors include material constitutive law (initial yield criterion, strain hardening, and hardening law), element type, contact model, friction law, and mesh density.

Typically, the study of the accuracy of springback uses test parts formed under industrial conditions. The friction and contacts, as well as the part geometry, generally result in membrane and shear stresses superimposed on the bending stresses, which makes the stress distribution complex. Since the theoretical models for these processes are mathematically involved, the traditional approach has been to compare FEA results with experimental validation. Comparison of the total springback can mask different errors that counteract one another. This makes it difficult to separate true accuracy from fortuitous coincidence. Since an exact solution exists only for pure bending of perfectly plastic materials, by comparing FEA results with theoretical results for the pure bending process, the performance of different element formulations, analysis parameters, and so on, can be objectively studied.

2.4. Present Study

Pure bending is selected as a candidate process that can be used as an objective test for comparing the performance of different FEA parameters in sheet forming and springback. Such tests can be used as good benchmark to identify the appropriateness of the results obtained by a particular combination of parameters in the analysis. Springback can be measured without error if an accurate bending moment is obtained from these analyses.

However, when a sheet made of a perfectly plastic material is bent, it is prone to developing a plastic hinge in the sheet. It requires the use of subroutines to enforce multi-point constraints on the sheet nodes in order to achieve uniform pure bending. This has been accomplished and sheets have been bent to a relative curvature of approximately 0.5. FEA results are compared with theoretical models and available experimental data. Comparing the bending moment given by FEA with that predicted by the appropriate theoretical solution reveals the accuracy with which the type of FEA and the input parameters used can represent states of pure bending.

The effect of the number of integration points, element formulations, convergence testing, and discretization is studied in this work.

CHAPTER 3

TECHNICAL APPROACH

Finite element analysis of uniform pure bending is used to compare different types of analyses and FEA packages for their springback prediction capability. Uniform pure bending is realized by applying a couple at one end of the sheet with symmetric boundary conditions on the other. The current study covers values of relative curvature ($\chi = t/r_m$) ranging up to 0.8, which is in the range of industrial bending operations. For these values of χ, FEA results of simulations with an elastic perfectly plastic material model are compared with Hill's analytical solution for perfectly plastic materials and FEA results for simulations with work-hardening material models, with the models of Crafoord (1970) and Dadras and Majlessi (1982).

3.1. Simulation of Uniform Pure Bending

The basic requirements for realizing uniform pure bending are as follows:

i. Bend the sheet using a pure bending moment.

ii. Do not use any shear forces, normal forces, or contacts with tooling to bend the sheet, since they lead to membrane and/or shear stresses in the sheet.

Various models were developed to realize different levels of pure bending. A detailed description of the development history is compiled in Appendix B.

In bending the outer layers of the sheet are subjected to tensile strain and the inner layers to compressive strain. To simulate a pure bending moment, two equal and opposite forces are applied on two adjacent nodes at one end (the right end, see Figure 7) of the sheet. As the sheet bends, the direction of action of these forces follows the rotation of the end face (right side) of the beam. Symmetric boundary conditions are applied to the other (left) end of the sheet. The left-most nodes of the sheet are constrained from moving in the X-direction. The central node in

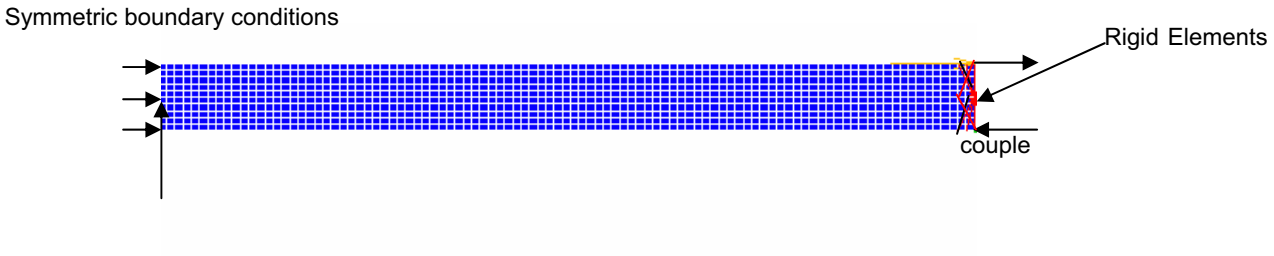

Figure 7. FEA model for 2 elements.

this set is also constrained from moving in the Y-direction. Figure 7 shows a schematic of the model.

The forces comprising the couple result in significant local effects on the elements near the nodes to which they are applied. This makes the convergence of non-linear iterations used in implicit solvers difficult. Rigid elements are used to prevent localized deformation and distribute the force over a larger area of the sheet. Rigid beam elements are intrduced from the nodes on which the couple forces are applied to other neighboring nodes, as shown in Figure 7, among the elements.

The sheet thickness used in each model is 4 mm. In this study of pure bending, the length of the beam is not a significant factor because uniform pure bending is independent of the length of sheet. Two–dimensional simulations are carried out using a variety of continuum elements, including 4–node and 8–node plane strain elements. Shell elements are used for 3D simulations. The z-displacement and the X and Y rotations of all the nodes in the model are constrained, as shown in Figure 8 in order to enforce plane strain conditions. Note that one row of elements along the X-direction would have been sufficient, though three are used.

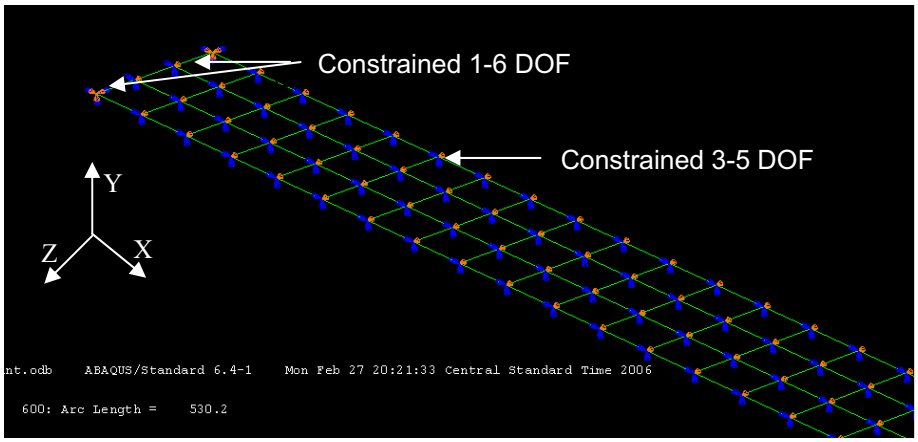

Figure 8. Boundary conditions for 3D simulations.

The Riks-Ramm loading procedure is used in the analysis. Although the moment required to bend the sheet initially increases with curvature, as the relative curvature approaches unity the moment required to continue bending decreases. The magnitude of applied couple should decrease at this time to avoid convergence errors. The Riks-Ramm procedure offers the required automatic loading stepping algorithm. It is typically used for snap-through problems where similar reduction of load with displacement is encountered. A brief description of the Riks-Ramm procedure, adapted from the MARC (2005) and ABAQUS theory manuals, is provided in Appendix C. Equivalent models are developed in MARC and ABAQUS for comparative analysis.

3.2. Analysis in MARC and ABAQUS/Standard

Both MARC and ABAQUS/Standard carry out the bending simulation by direct (implicit) time integration. The 2D plane strain analyses in MARC are carried out using fully integrated plane strain Quad4 elements and Quad8 elements (element types 11 and 27 in MARC, respectively). Quad4 elements employ linear interpolation functions, while Quad8 elements employ quadratic interpolation functions to calculate the displacements based on the nodal values. MARC element 75, a four node, thick shell element with global displacements and

rotations as degrees of freedom (MARC manual, Vol. B, 2005) is used in the 3D model with shell elements.

For the 2D plane strain models in ABAQUS, CPE4 and CPE8 element formulations (equivalent to Quad4 and Quad8 elements in MARC) are used. S4 elements are used for simulations with shell elements. They include *assumed strain* formulation to avoid shear locking. S4R, CPE8R and CPE4R elements are used in ABAQUS to study the effect of reduced integration.

3.3. Material Properties

FEA results are validated with the exact theoretical model given by Hill (1950) for a perfectly plastic material property. A material with a constant yield stress of 58.1 MPa is used in the perfectly plastic simulations. Because the theory assumes a rigid, perfectly plastic material, an analysis was carried out with the Young's modulus scaled up by a factor of 10 to determine the effect of reduced elastic strains.

FEA results obtained using the work-hardening materials are compared with the models given by Crafoord (1970) and Dadras and Majlessi (1982). The same effective stress vs. effective strain curve is used in computing the bending moment according to both these models.

The Voce (1948) equation for material properties is

$$\overline{\sigma} = A + B\overline{\varepsilon} - Ce^{-D\overline{\varepsilon}} \tag{3}$$

where the constants for aluminum are A = 131.6, B = 32.2, C = 73.5, and D = 3.75, as given by Crafoord (1970).

Dadras and Majlessi (1982) use Ludwik's rigid work hardening material law which can be stated as

$$\sigma = \sigma_y + \mathrm{K}\varepsilon^n \tag{4}$$

TABLE 1

COEFFICIENTS OF LUDWIK MATERIAL MODEL THAT REPRESENT THE BEHAVIOR OF ALUMINUM AS SHOWN IN FIGURE 9.

Material	Young's Modulus (MPa)	Initial Yield Stress (MPa)	Strength Coefficient (MPa)	Poisson's Ratio	Strain Hardening Exponent
Aluminum	72.942	53.15	145.02	0.35	0.665

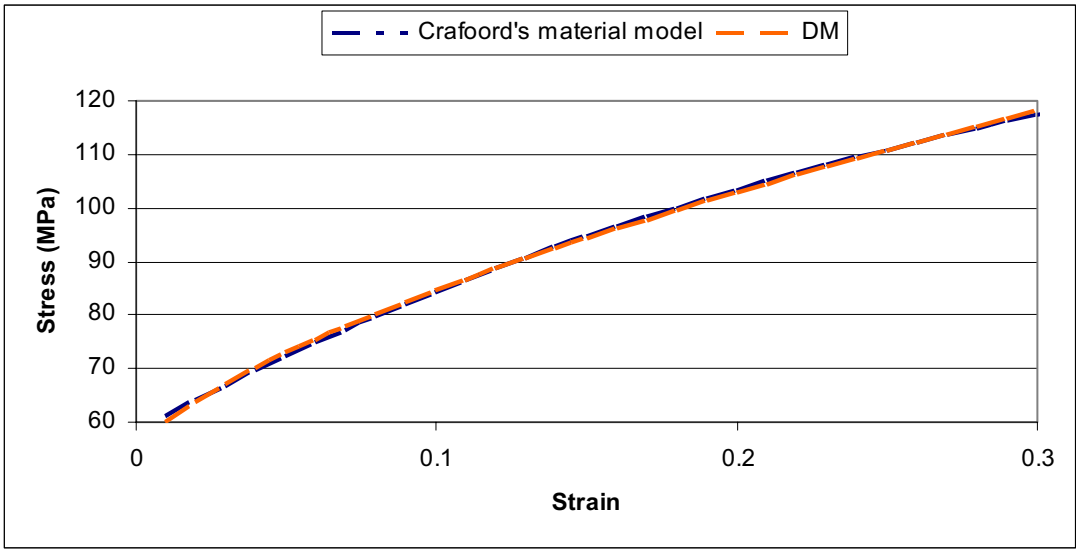

Figure 9. Stress-strain curve of aluminum represented using the Voce equation.

Equivalent parameters for both these models to represent the same strain hardening curve are obtained by curve fitting. In the sheet bending operations considered, the maximum strains reached are about 0.3. Hence the curves are fit to this value of strain, which can be noted in Figure 9. The coefficients of Ludwik model corresponding to the coefficients of the Voce model shown below equation 3 are listed in Table 1.

3.4. Multi–Point Constraints for Uniform Bending of Perfectly Plastic Sheets

Perfectly plastic materials are prone to developing *plastic hinges* caused by plastic instability. Plastic hinging in bending is comparable to the necking in tension tests.

In this study, multi-point constraints are employed to constrain the nodes along the central fiber of the sheet to lie on a circle. As noted earlier, the first node (on the left side) along the center fiber is subject to symmetric boundary conditions. The second node is free to move as dictated by the loading. All the nodes on the central fiber of the sheet to the right of the second node follow the deformation of the second node. This is achieved by using user subroutines – "UFORMS" in MARC and "MPC" in ABAQUS. The following is a succinct explanation of the governing equations for the subroutine. Figure 10 shows a diagrammatic representation for the derived equations.

The equations specified in the user subroutine need to constrain the movement of the nodes in the central row of the beam to appropriately scale and follow the movement of the second node (Node 2) of the same row. Given the displacement of Node 2, the radius, *R*, can be calculated using the formula

$$R = \frac{L\cos\theta_1}{\sin 2\theta_1} \tag{5}$$

The length *L* of the segment between Node1 and Node2, is given by

$$L = \sqrt{((x_2 - x_1)^2 + (y_2 - y_1)^2)} \tag{6}$$

and the angle θ_1 is calculated as

$$\theta_1 = \tan^{-1}\left(\frac{y_2 - y_1}{x_2 - x_1}\right) \tag{7}$$

$$x_i = X_i + u_i \tag{8}$$

$$y_i = Y_i + v_i \tag{9}$$

where x_i and y_i denote the current coordinates of the node indicated by the subscript i, X_i and Y_i denote the original coordinates, and u_i and v_i denote the displacements in the X and Y directions respectively.

Node 1 is constrained in X and Y directions, and in the FEA model used, is also located at the origin of the coordinate system. This simplifies the formulae of L and θ_1 as shown below:

$$L = \sqrt{x_2^2 + y_2^2} \tag{10}$$

$$\theta_1 = \tan^{-1}\left(\frac{y_2}{x_2}\right) \tag{11}$$

Uniform bending requires that the nodes on the central row be equally spaced, and that at all subsequent nodes after Node 2 be placed at an angular increment of $2\theta_1$ about the center of curvature, as shown in Figure 11. The X and Y coordinates of any node i (along the central row) can be obtained using

$$x_i = R\sin(2i\theta_i) \tag{12}$$

$$y_i = R(\cos(2i\theta_1) - 1) \tag{13}$$

A plot of the coordinate locations obtained from these equations (at fixed θ_1) for all the nodes in the central row (initially at Y = 0) is shown in Figure 11. It validates the equations to be able to provide the appropriate constraints when used in the subroutine to realize uniform bending. Note that Node 2 is free to move, and its movement forces the other centerline nodes to move appropriately, resulting in a uniform bend along the length of sheet. The reaction due to the applied MPCs is not expected to be large because it just takes a gentle guidance to have the sheet continue to bend uniformly. Furthermore, the constraint equations do not constrain the radius of curvature of bend and are not expected to cause any significant reaction forces on the sheet.

These equations have been incorporated in the MPC subroutine (for ABAQUS) and UFORMS subroutine (for MARC).

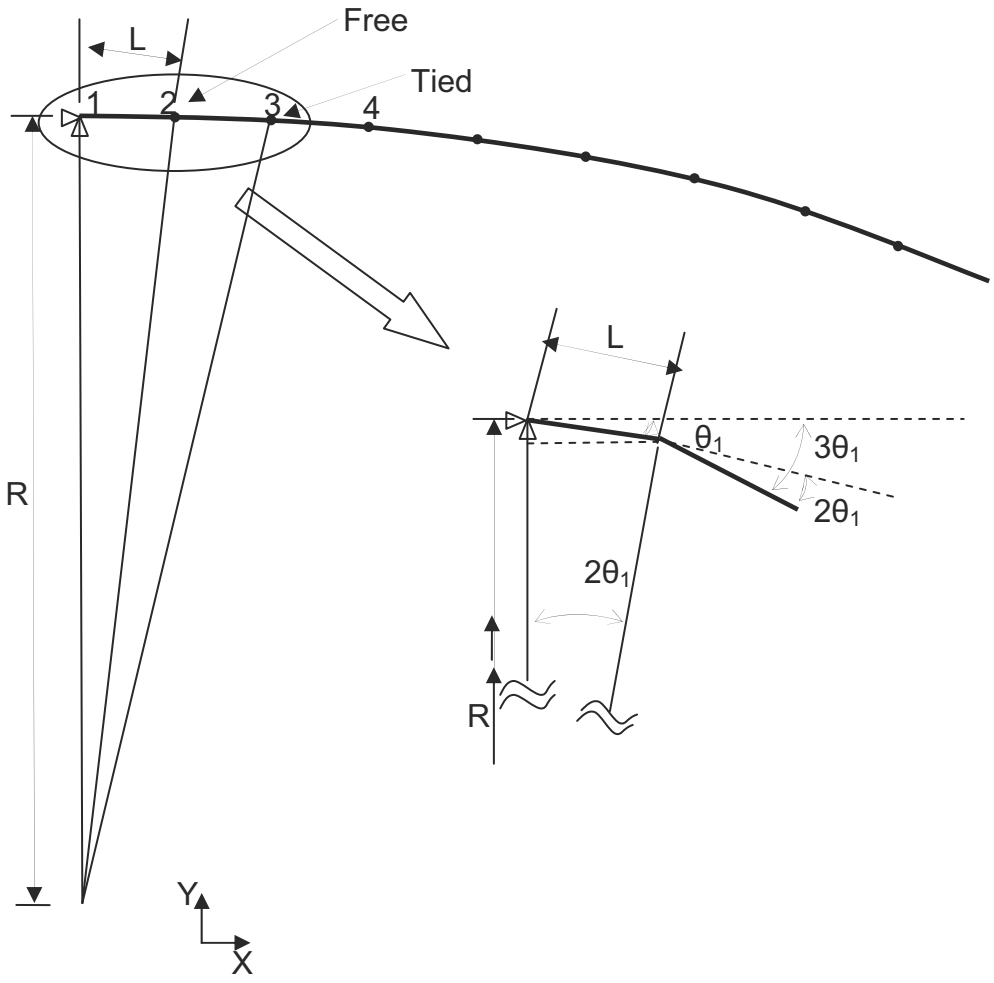

Figure 10. Geometric relationships between the location of the free node and the other nodes along the centerline of the sheet, used in deriving the constraint equations on the centreline nodes of the sheet.

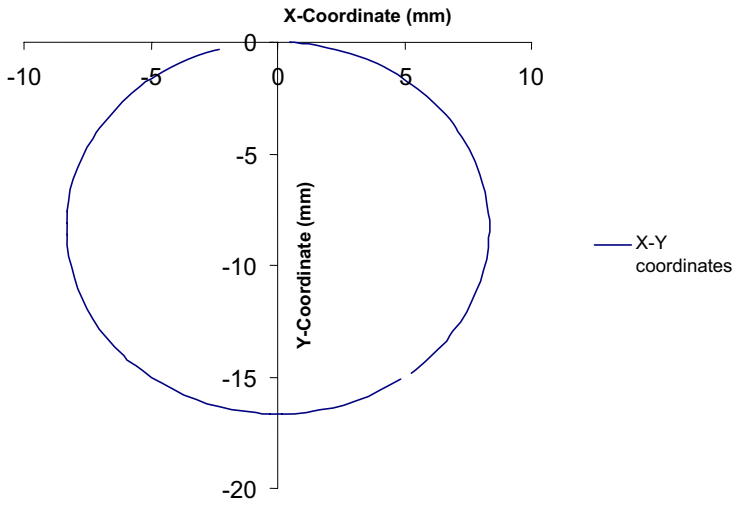

Figure 11. Plot of the nodal positions given by the constraint equations (calculation in MAPLE), at an intermediate stage in the bend showing that the equations would indeed constrain the nodes to lie on a circle.

3.5. Results Post Processing

Post-processing of the results for each of the simulations is performed using Microsoft Excel. The uniformity of bend is verified by fitting a circle through the coordinates of the first 70 nodes along the central row. The center of the circle is the center of curvature of the sheet, from which the radial and angular locations of each of the nodes is defined and used in subsequent computation. The stress components in the coordinate directions are transformed to the circumferential stresses and radial stresses according to

$$\sigma_{\theta\theta} = \sigma_{xx} \cos^2\theta + 2\sigma_{xy} \sin\theta \cos\theta + \sigma_{yy} \sin^2\theta \tag{14}$$

$$\sigma_{rr} = \sigma_{xx} \sin^2\theta + 2\sigma_{xy} \sin\theta \cos\theta + \sigma_{yy} \cos^2\theta \tag{15}$$

The total bending moment per unit width into the plane is obtained by integrating (summing) the action of the tangential stresses through the thickness of the sheet as follows:

$$M_B = \int_{r_i}^{r_0} \sigma_{\theta\theta}.r.dr = \int \left[\sigma_i + \left(\frac{\sigma_{i+1} - \sigma_i}{r_{i+1} - r_i} \right)(r - r_i) \right].r.dr \tag{16}$$
$$= \sum_i \left[\frac{(\sigma_i + \sigma_{i+1})}{2}(r_{i+1} - r_i)\left(\frac{r_{i+1} + r_i}{2} \right) + \frac{1}{12}(\sigma_{i+1} - \sigma_i)(r_{i+1} - r_i)^2 \right]$$

Figure 12(a) represents the parameters involved in this calculation. Figure 12(b) represents the procedure schematically. The resulting summation shown above can be arrived at either by performing the integration or by considering individually the contributions of the mean stress over a segment and the gradient of stress over it, as shown in Figure 12(a).

$$\begin{aligned} \int \sigma_{\theta\theta} r dr &= \int_{r_i} \sigma_i + \frac{(\sigma_{i+1} - \sigma_i)}{\Delta r}(r - r_i) r dr \\ &= \int_r^{r_{i+1}} \sigma_i r dr + \int_r^{r_{i+1}} \frac{(\sigma_{i+1} - \sigma_i)(r - r_i)}{(r_{i+1} - r_i)} r dr \\ &= \sigma_i \frac{r^2}{2}\Big|_{r_i}^{r_{i+1}} + \frac{\sigma_{i+1} - \sigma_i}{r_{i+1} - r_i}\left[\frac{r^3}{3} - \frac{r_i r^2}{2} \right]\Big|_{r_i}^{r_{i+1}} \\ &= \frac{\sigma_i}{2}\left[r_{i+1}^2 - r_i^2 \right] + \frac{\sigma_{i+1} - \sigma_i}{r_{i+1} - r_i}\left[r_{i+1}^2 \left(\frac{r_{i+1}}{3} - \frac{r_i}{2} \right) + \frac{1}{6} r_i^3 \right] \end{aligned} \tag{17}$$

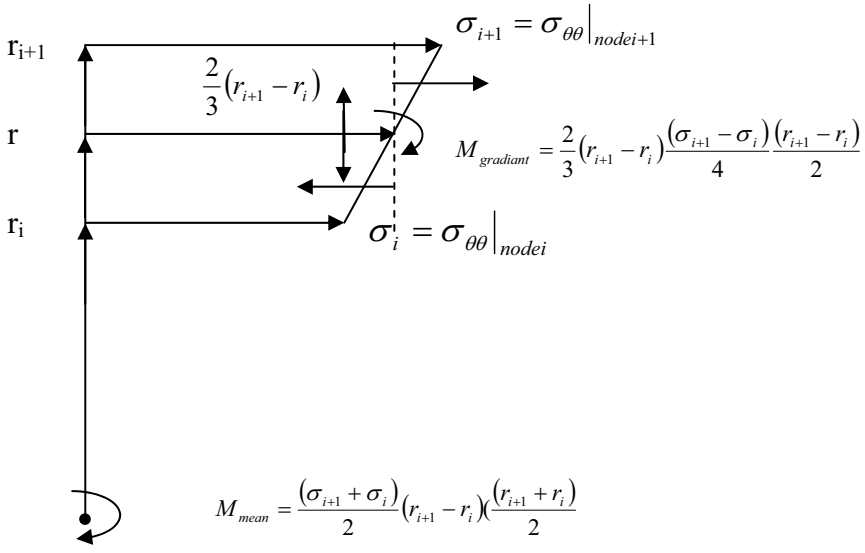

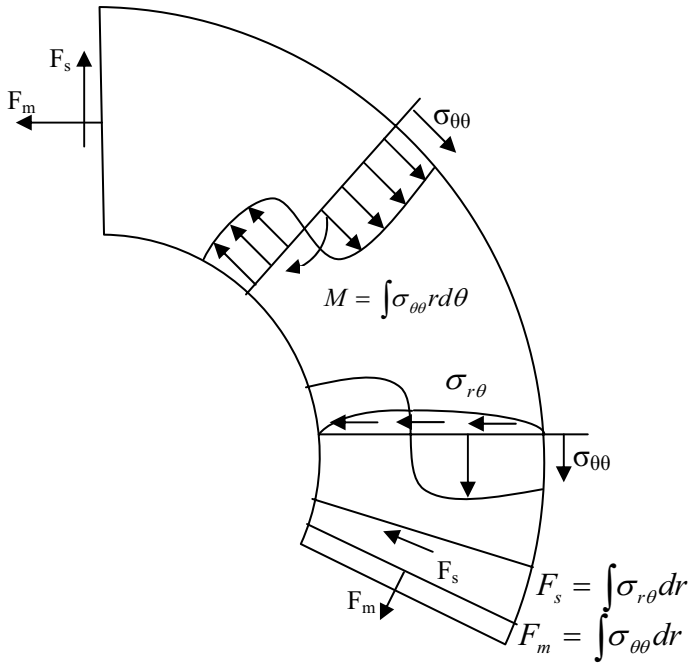

Figure 12(a) Parameters to calculate moment; (b) Schematic describing results post-processing to obtain the bending moment, membrane force and shear force at each section by summation of relevant moment and stresses over the cross-section.

The stresses are also summed up over each of the sections to obtain the total membrane and shear forces.

$$F_m = \int_{r_i}^{r_o} \sigma_{\theta\theta}.dr = \sum_{i=1}^{n} \frac{\left(\sigma_{\theta\theta i} + \sigma_{\theta\theta i+1}\right)}{2}(r_i - r_{i-1}) \tag{17}$$

$$F_f = \int_{r_i}^{r_o} \sigma_{r\theta}.dr = \sum_{i=1}^{n} \frac{\left(\sigma_{r\theta i} + \sigma_{r\theta i+1}\right)}{2}(r_i - r_{i-1}) \tag{18}$$

If the membrane force is non-negligible, the true bending moment is obtained by subtracting the contribution of the membrane force from the moment calculated in equation 16 as follows:

$$M_{FEA} = M_B - F_m r_n \tag{19}$$

The values of M_{FEA}, F_m and F_s are averaged over cross-sections 10 through 70 to obtain the average M_{FEA}, F_m and F_s which are used for further processing. Moments for the shell

elements are output by the software. An average of these moment values over nodes of the sheet is calculated and used as the value of bending moment.

The same processing is repeated for the results obtained at the end of the springback simulation. The curvature after springback is obtained by fitting a circle to the centerline nodes. The residual moment, membrane force, and shear force are also obtained as described above.

Subsequently, after post-processing, the error in bending moment calculation is obtained. Springback depends directly on the calculated bending moment. A systematic method of error analysis in springback prediction is discussed in the following section.

3.5.1. Error Analysis

The change in angle due to springback is directly related to the change in curvature by the relation $\Delta\theta = \Delta\kappa * BA$, where BA is the bend allowance, the length of the unstretched fiber, which, by definition, remains constant. The total error in springback prediction by FEA can be partitioned into the following separate errors:

1. Error in the bending moment required for forming at the forming stage.
2. Error during the unloading stage, if the sheet does not unload completely.
3. Error in change in curvature of the structure in response to the unloading of the bending moment, as compared to the change in curvature expected theoretically.

These three error components are defined as

$$E_1 = \frac{\mathrm{M}_{\mathrm{FEA}} - \mathrm{M}_{\mathrm{theory}}}{\mathrm{M}_{\mathrm{theory}}} \times 100\% \tag{20}$$

$$E_2 = -\frac{\mathrm{M}_{\mathrm{r}}}{\mathrm{M}_{\mathrm{theory}}} \times 100\% \tag{21}$$

$$E_3 = \frac{\Delta\kappa_{FEA} - \Delta\kappa_{theory}}{\Delta\kappa_{theory}} \times 100\% \tag{22}$$

where $\Delta\kappa_{theory} = \frac{|M_{springback}|}{E'I}$ M_r is the residual bending moment after springback, M_{theory} is the bending moment expected based on theory, M_{FEA} is the bending moment computed from FEA results as described in the previous subsection and $M_{springback}$ is given by:

$$M_{springback} = \left(\frac{2}{2+n}\right)\left(\frac{wK'}{r_c^n}\right)\left(\frac{t}{2}\right)^{2+n} \tag{23}$$

It can be seen from the above definitions that the total error, $E=E_1+E_2+E_3$ is the ratio of the error in springback angle prediction to the actual springback angle. A negative E indicates less springback than theoretical results, while a positive value of E indicates a higher springback as compared to theory.

The $\Delta\kappa_{theory}$ obtained using the above mentioned equation is true for straight beams and is not accurate for curved beams, especially of higher curvatures. A more accurate theory proposed by Timoshenko and Goodier (1970) is used to calculate the change in curvature of the bent sheet ($\Delta\kappa_{theory}$). This is explained in detail in Appendix E.

CHAPTER 4

RESULTS AND DISCUSSION

4.1. Verification of Uniform Pure Bending

The sheet is found to bend uniformly under the effect of the applied couple and constraint equations. Figure 13 shows the position of the centerline nodes of the sheet with increase in bend curvature (i.e. the geometry of the central layer of the bent sheet at different time increments), as obtained from finite element analysis. The change in thickness of the sheet with bending is also shown in the legend.

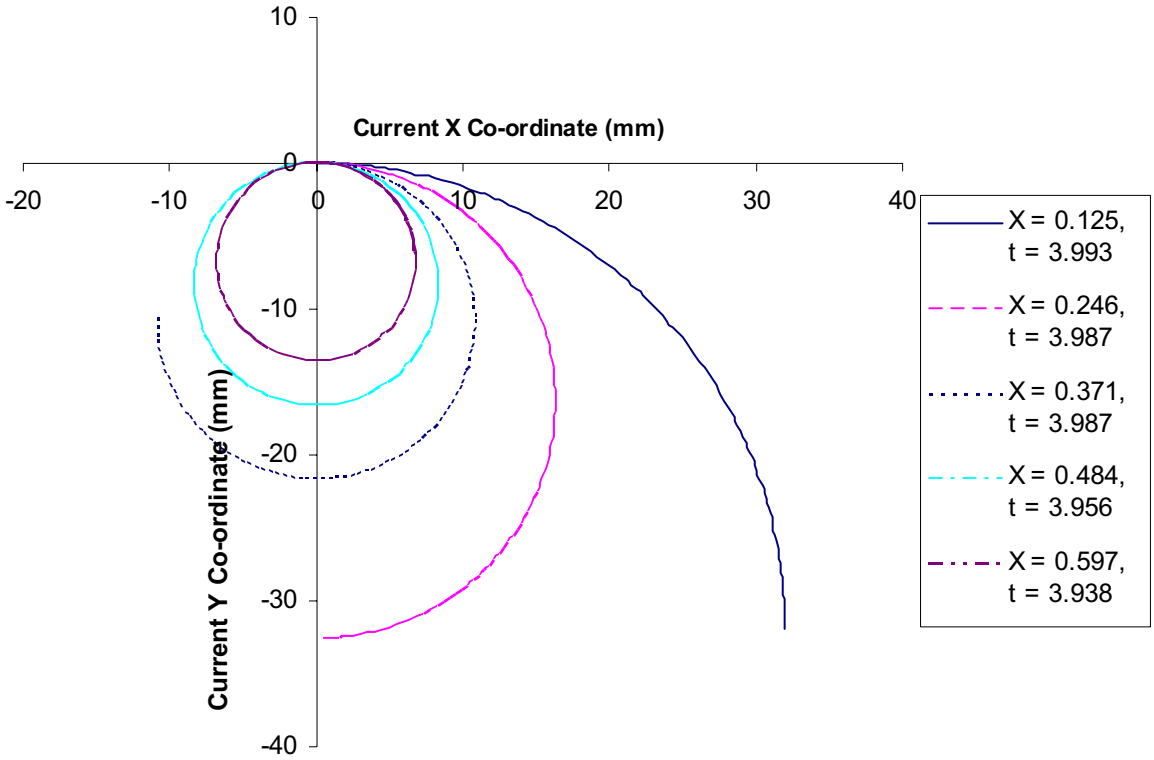

Figure 13. The curvature of the centerline nodes of the sheet at different stages of bending. (condition corresponding to simulation J in Table 4).

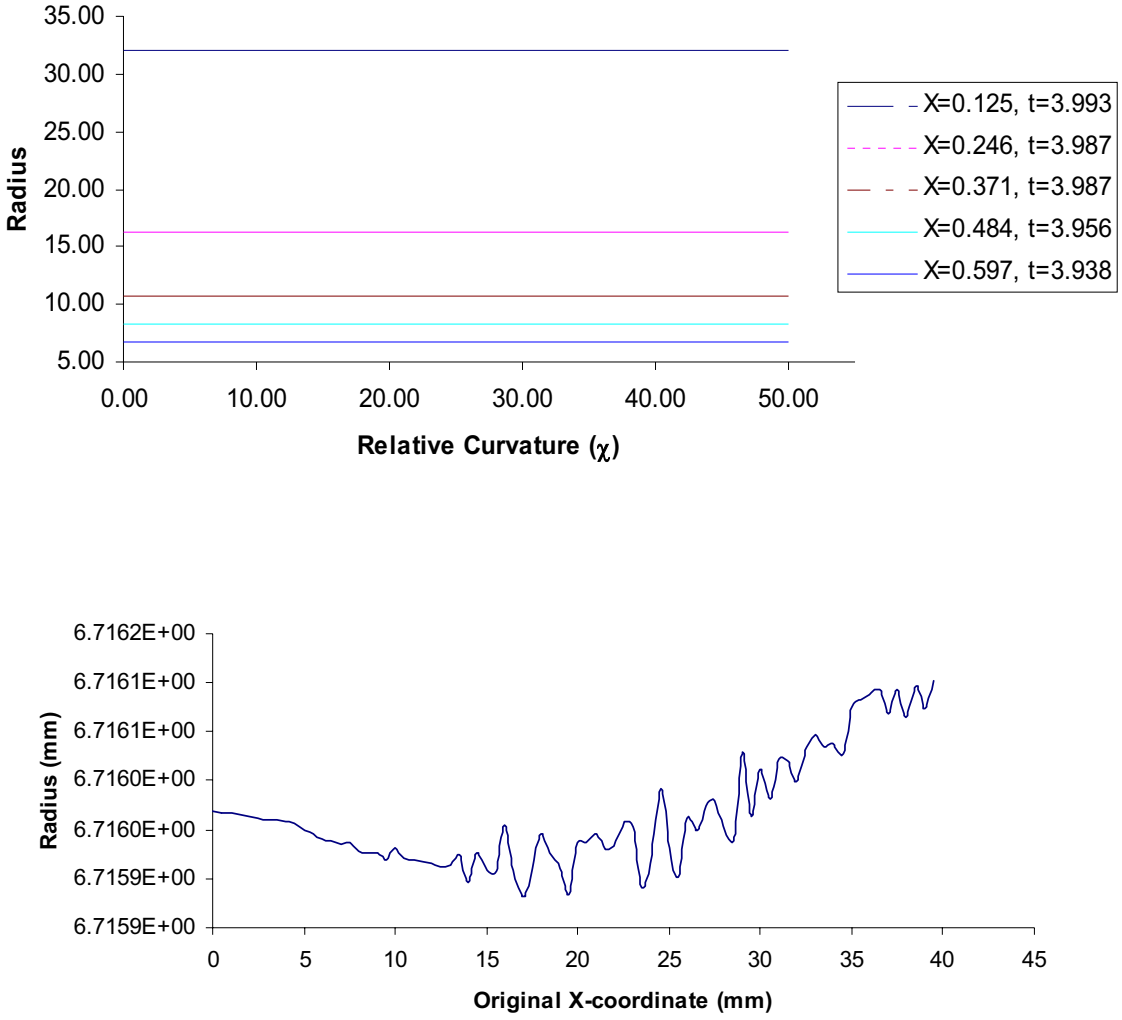

Figure 14(a). The radius of curvature of centerline nodes with increase in χ, (b) radius of the centerline nodes at $\chi = 0.597$.

Figure 14(a) shows the variations in calculated radii along the centerline nodes of the sheet. Figure 14(b) shows the variations in a magnified manner for the tightest bend in figure (a) to show that the deviation from a true circle is negligible. The standard deviation for this set of calculated radii at different sections is 0.003 mm.

Figures 15(a) and 15(b) show typical distributions of maximum principal stress along the sheet for simulations with 2D (4-noded) and 3D (4-noded) elements and highlight the fact that the stresses are also uniform around the bend.

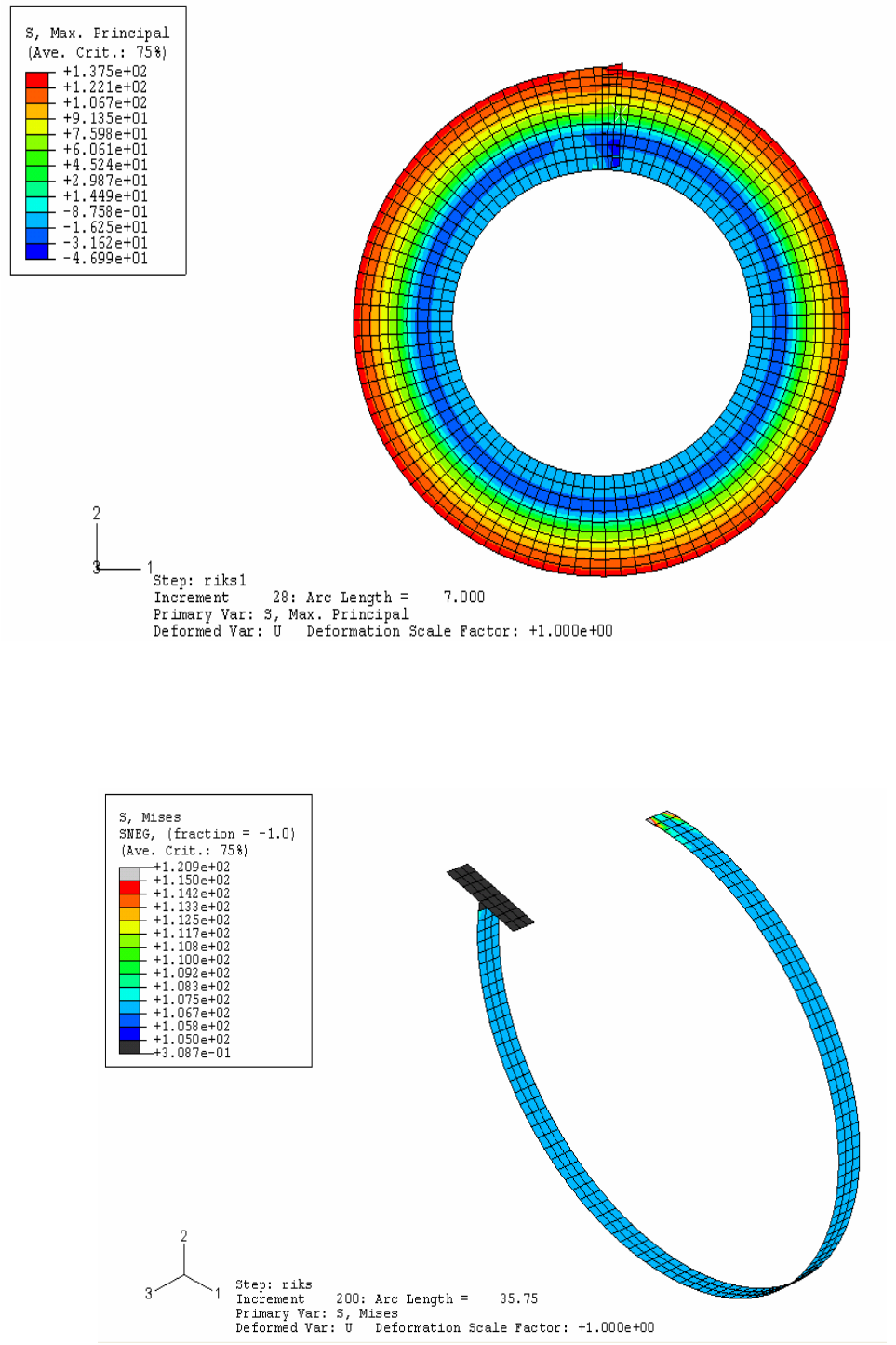

Figure 15(a). Maximum principal stress (2D elements); χ=0.484. (Condition corresponding to simulation J in Table 4); (b)Maximum principal stress (3D shell elements); χ=0.36. (condition corresponding to simulation R in Table 4).

Figure 16 shows the distribution of circumferential and radial stress through the thickness of the bent sheet. The circumferential stress is found to follow the pattern of stress-strain model of the material as proposed by Dadras and Majlessi (1982). The radial stress is compressive throughout the thickness of the sheet, but show some deviation from the distribution expected based on theory.

4.2. Comparison of FEA Results for Perfectly Plastic Material with the Predictions of Hill's Model

Using the approach mentioned in the previous chapter, uniform pure bending has been carried out under the conditions mentioned in Table 2 (page 37) for elastic perfectly plastic material. The changes made to the model between one analysis and the next (referred to by the next index and listed in the row below) are highlighted in these tables. For instance, in Table 2, it can be seen that the effect of three different convergence tolerances are investigated in analyses A and B, for CPE4 and CPE4R elements subject to couple forces while F and G corresponds to analyses with S4 and S4R elements subjected to moment loads.

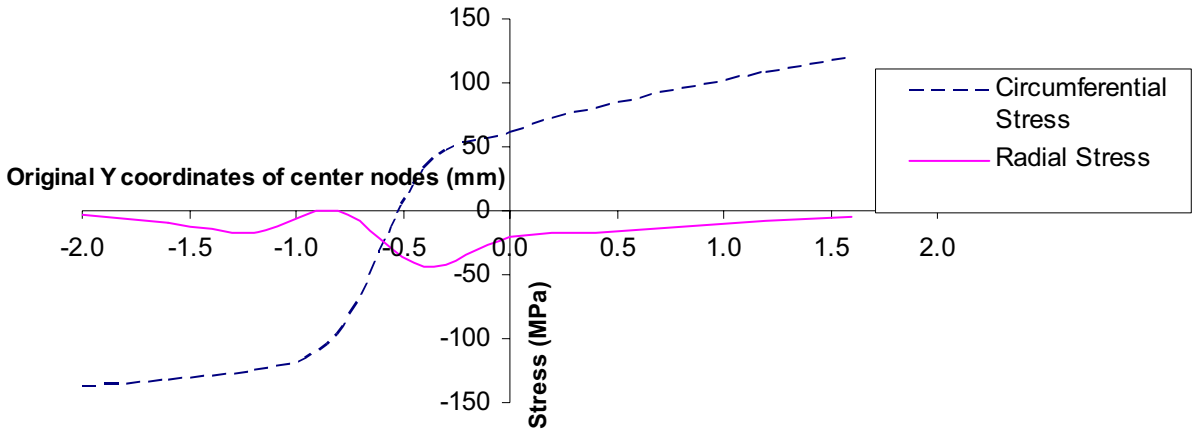

Figure 16. Circumferential and radial stresses (averaged over the first 70 sections) induced along the thickness of the sheet (simulation J in Table 4).

Figure 17 shows a comparison of the bending moment given by ABAQUS with that given by Hill's model for perfectly plastic materials. With all plane strain element simulations, the bending moment is correct to within 3% of the theoretical value up to a relative curvature of 0.3. The simulation with E increased ten times (simulation C in Table 2), to study the effect of rigid perfectly plastic material, did not show much difference in the results at lower χ values ($\chi <$ 0.4)), although the bending moment increased steeply at higher values of χ (> 0.4). The change in thickness of the sheet for a perfectly plastic material is shown in Figure 18. The thickness change is about 0.5%. Simulations F and G use fully integrated and reduced integrated shell elements respectively and show an error close to -10%. The error increases to about 37% for these elements when a coarser discretization with only 4 and 9 elements along a 90 degree bend is used (simulation H and I).

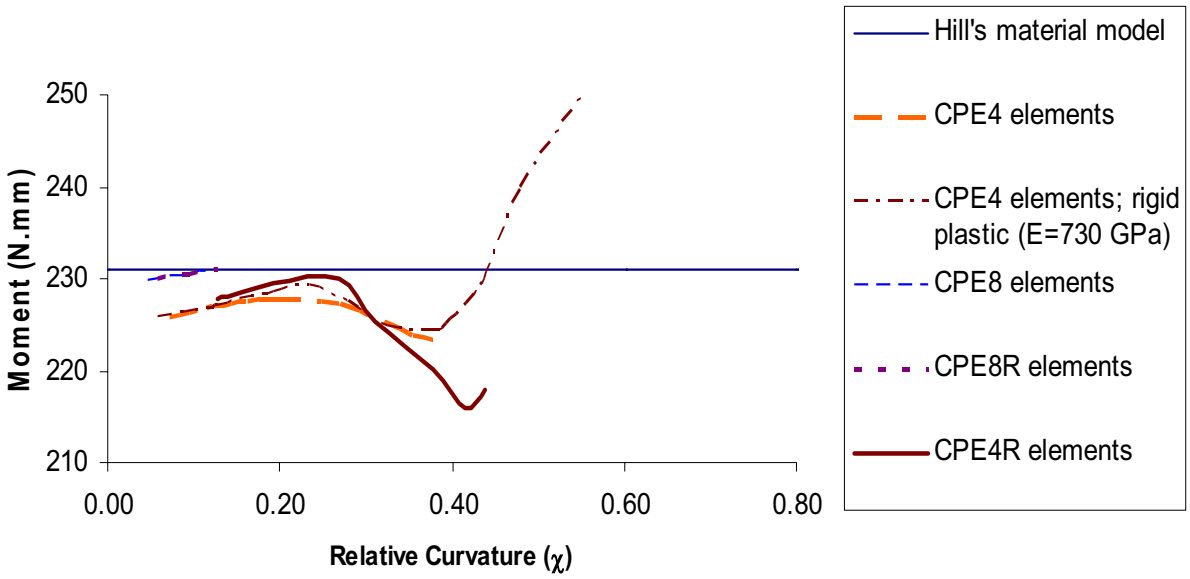

Figure 17. Comparison of the variation of moment with relative curvature given by FEA with the theoretical model of Hill (1950).

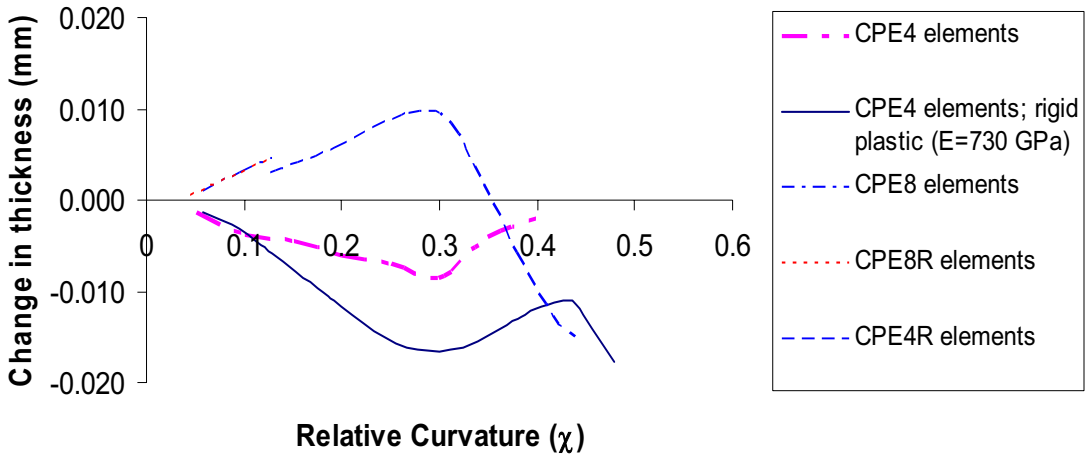

Figure 18. Comparison of the variation in sheet thickness with relative curvature given by ABAQUS using five different element types, with the constant sheet thickness expected based on the theoretical models of Hill (1950).

Table 3 (page 38) shows results of these analyses with ABAQUS. The CPE4 and CPE4R elements do not show much difference in bending moment at χ close to 0.3. The CPE4 elements show a negative error of about 3% in bending moment, indicating a lower bending moment than that determined by theory which will lead to reduced springback. The 8-noded plane strain elements show an error close to 0% at very low curvatures. The 3D shell element shows a negative error of about 10%. As the discretization of the sheet is made coarser, the error in bending moment rises to about 37%. The lower bending moment predicted by FEA under most conditions also indicates under prediction of springback.

4.3. Comparison of FEA Results with Theoretical Models for Work-Hardening Materials

Figure 19 shows the relationship between normalized moments and relative curvature for work-hardening material obtained from ABAQUS. CPE8 and S4R elements show values close to Crafoord's model at lower χ, while the deviation increases with increasing χ. S4R elements are able to attain high curvatures with χ nearing 1.0; however, at higher curvatures, S4R elements

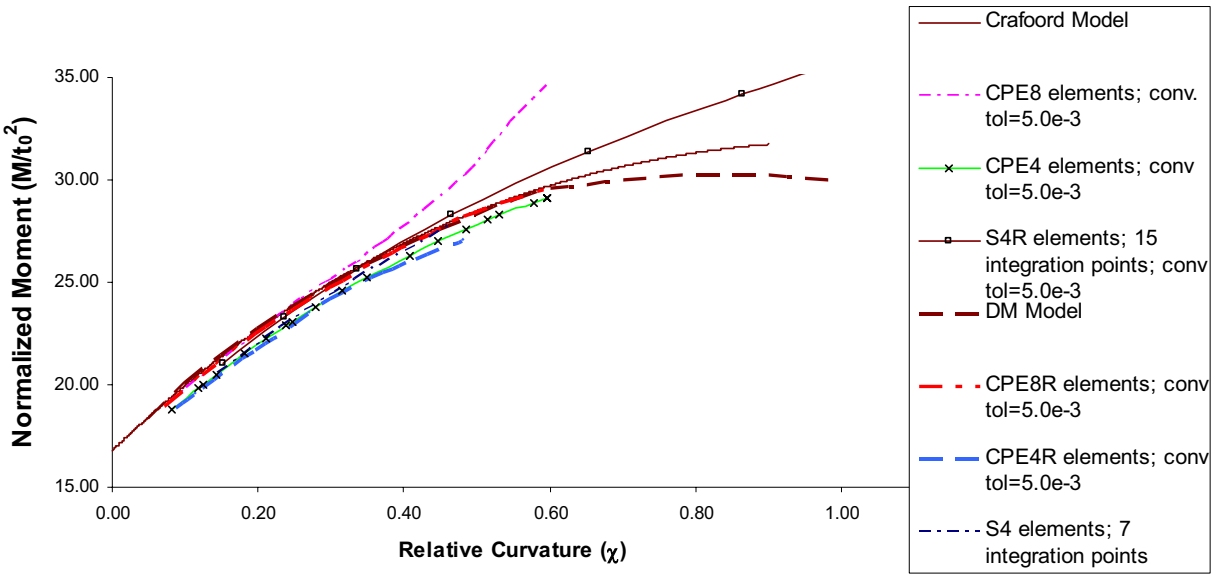

Figure 19. Comparison of the variation of moment with relative curvature given by ABAQUS using five different element types, with the theoretical models of Crafoord (1970) and Dadras and Majlessi (1982).

show increased bending moment values compared to the theoretical models. CPE4 elements show a good accuracy in calculating bending moment. The total error values obtained are about -5% indicating a smaller springback prediction for simulations. In all, close correlation is obtained using 4 noded plane strain elements. The reduced integration and full integration elements display similar results other then a minor deviation of about 1% at curvatures close to 0.5.

Figure 20 shows the variation of sheet thickness with increasing curvature. It shows a good correlation with Crafoord's theoretical model. The decrease in thickness is steady as the curvature increases. As the moment calculation is directly proportional to the square of thickness, the decrease in thickness reduces the total calculated moment. The S4R elements show constant thickness of 4mm. 4 noded and 8 noded elements show similar trends, although the CPE4 and CPE4R elements are close to the theoretical results.

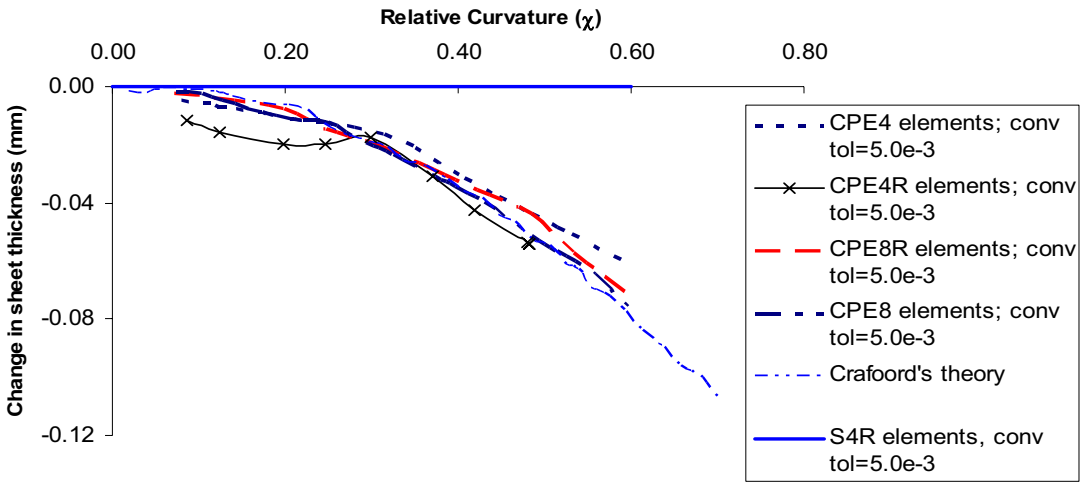

Figure 20. Comparison of the variation in sheet thickness with relative curvature given by ABAQUS using five different element type, with the theoretical models of Crafoord (1970).

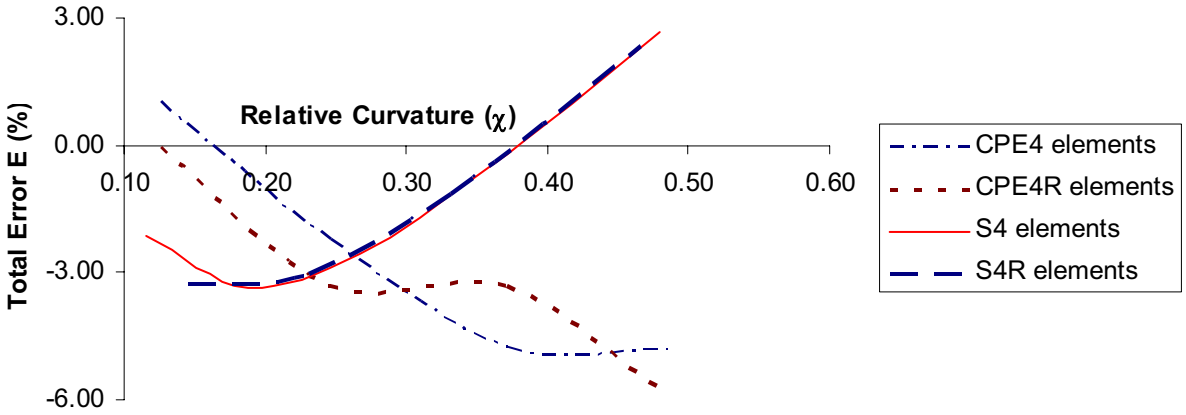

Figure 21. Comparison of Total error (E) with relative curvature predicted by ABAQUS using four different element types.

Figure 21 shows the total error as the sheet bends to higher curvature. 2D plane strain elements show an error trend going from positive error towards negative error indicating a higher probability of under-estimating springback at higher curvatures, while the reverse is obtained for 3D shell elements where the error increases with the increase in curvature, likely attributable to the fact that the thickness of the shell elements remain constant.

Figure 22 is a plot of the normalized bending moment with χ for the work-hardening material using MARC software. Similar to ABAQUS, the 2D 4-noded elements give close results at lower χ, while the deviation from theory increases with increase in curvature. 3D fully integrated shells show a close approximation to theory at lower curvatures but the error increases at higher curvatures. The simulation with user subroutine shows a peak in calculated bending moment at χ close to 1.1 and decreases sharply beyond this. The trend is in line with theoretical results where the moment decreases after χ increases beyond 1. The plane strain elements show an error of about 15% as compared to the theoretical models.

Hence, it is seen that element type 11 in MARC and CPE4 elements in ABAQUS show a close correlation with the theoretical model. Element type 75 very closely follows the theoretical model until a relative curvature of 0.6. Beyond that, similar to S4R elements in ABAQUS, the bending moment predicted by them is greater than the theoretical models.

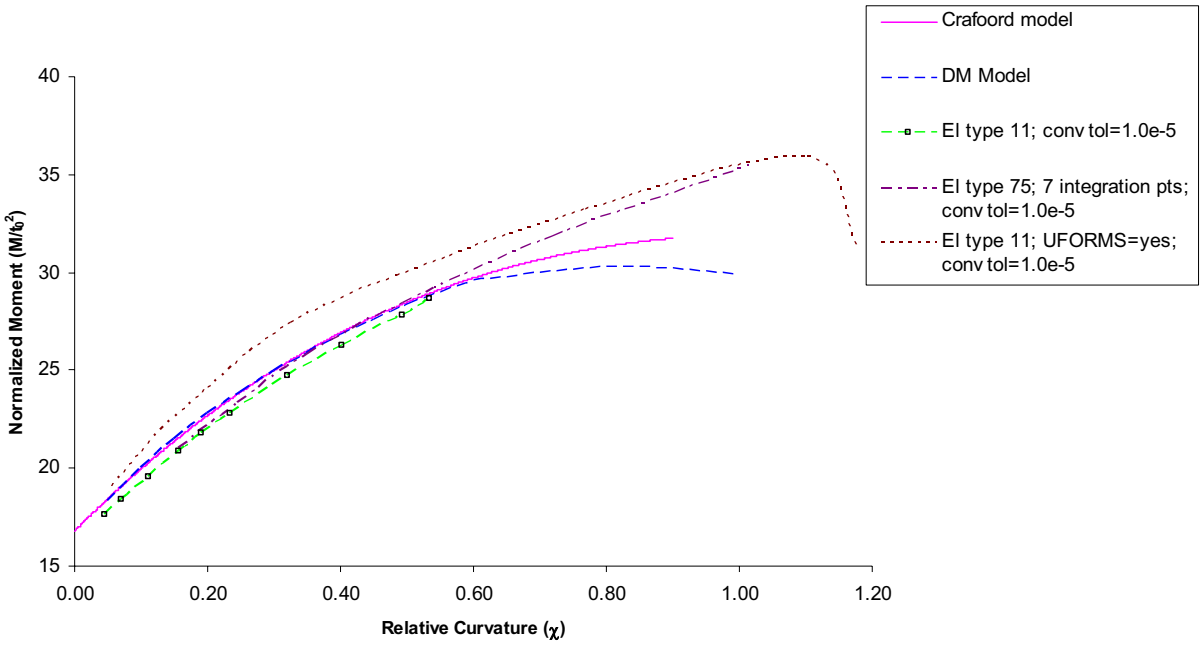

Figure 22. Comparison of the variation of moment with relative curvature given by MARC using three different element types, with the theoretical models of Crafoord (1970) and Dadras and Majlessi (1982).

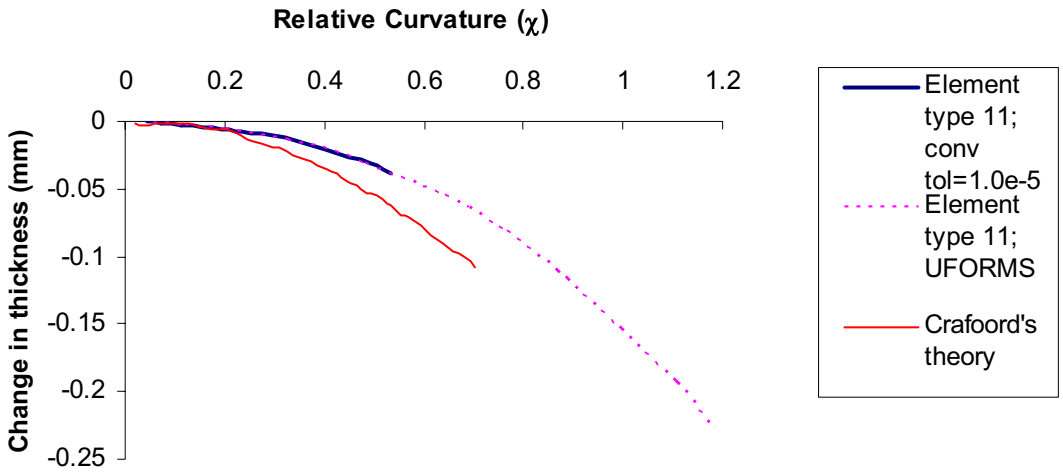

Figure 23. Effect of the user subroutine on the change in sheet thickness given by MARC.

Figure 23 shows the effect of using subroutine on the change in sheet thickness. It can be noted that the thickness variation between the two simulations is not significant. However, consistently decreasing trend deviates about 5% from the theoretical results at a χ of 0.6. The decreasing sheet thickness trend continues at higher curvature for simulation with subroutines.

Table 4 (page 43) lists the simulations carried out in ABAQUS, with different element formulations, number of integration points, discretization levels, loading types, and convergence tolerance values for work-hardening materials. Table 7 (page 46) is a similar list for simulations carried out in MARC. Different analysis inputs are chosen such that the comparison of the results for bending moment, completeness of unloading, and correlation between changes in curvature and unloading will provide a clear indication of the effect of changes in these parameters on the error in springback prediction.

The results for analyses with ABAQUS 2D 4-noded and 8-noded elements are shown in Table 5 (page 44) while Table 6 (page 45) shows the results for 3D shell elements. Similarly, Table 8 (page 47) shows MARC results for 2D elements while Table 9 (page 48) shows results for 3D fully integrated shell elements.

The results from Table 5 indicate an under-prediction of springback angle using the 2D elements. E_1 is about 2% for CPE4 elements (simulations J, K and L), indicating a good correlation with theory. E_1 is about -6% for CPE8 elements (simulations M, N and O) indicating smaller springback calculation. The simulation with CPE4 and higher discretization (Simulation Q) show an E_1 of less than 2%. E_2 for the 4-noded 2D elements (simulations J, K and L) is less than -1%, while it is about -9% for equivalent cases with CPE8 elements (simulations M, N and O). E_3 for mostly all the simulations with plane strain elements result in less than -10% errors (simulations J through Q except Simulation K). The section stress before springback for 4-noded elements is about 3% of the yield stress of the material (simulations J, K and L), while it is more than 10% for CPE8 elements (simulations M, N and O). Total error is negative for all the examined cases. The total error in actual calculation of springback is about -12% for CPE4 elements (simulations J, K and L), while it is about -20% for CPE8 elements (simulations M, N and O), indicating an under-prediction in bending moment calculation. An increase in convergence tolerance by 100 did not vary the result by more than 2% (simulations J, K, L and M, N, O).

Table 6 shows a comparison of results for 3D shell elements with full and reduced integration for different numbers of integration points. E_1 is about 4% for most of the cases with S4 and S4R elements (simulations R through AG except simulation Z). E_2 for all the simulations with 3D shell elements is less than 0.1%, indicating a complete unloading of the sheet. E_3 for S4R elements ranges between 2% and 10% (simulation R through AA) in the negative direction for most of the cases, while it is less than -2% for most cases using S4 elements (simulations AB through AG). Overall, the shell elements with reduced integration give an under-prediction of springback and show a negative error value for the simulations with different integration points

(simulation R, S, V, W), while shells with full integration show a positive total error of about 3% (simulations AA through AG except simulation AC), indicating a higher springback than predicted by theory. Similar to plane strain elements discussed previously, S4R elements do not show a difference in results by changing the convergence tolerance by a factor of 100. The moment loading in simulation T show a negative total error -11% indicating under-prediction of moments.

In Table 8, the 2D plane strain 4-noded and 8-noded elements in MARC, E_1 is about -3%, while E_2 is about -1%. E_3 shows a negative error of about 7% (simulation AH, AI and AJ). The membrane stresses after unloading for element 11 are about 5% of the initial yield stress, while they are about 14% for element 75. The change in overall error between simulations AH, AI, and AJ is not more than 2%, indicating a smaller influence of change in convergence tolerance for these analyses.

Table 9 shows an error estimate results for using 3D shell elements in MARC and varying the number of integration points through the thickness of the element. E_1 is less than 7% for most of the cases except simulation AP (with 11 integration points and tighter convergence tolerance), where the error is close to 16%. With a smaller E_2, a fairly good unloading, about 2% is seen in all cases. Simulation AG (with 5 integration points) and AP show an increased error in E_3. For other cases, the error is found to be less than 4%. The least overall error is predicted by element 75 with 7 integration points.

The 2D plane strain elements closely approximate the bending process. An error value of about -6% is found for the first stage. At lower curvatures, the FEA closely approximates theory. As curvature increases, the bending moment calculation deviates from the theory. Within shell elements, the reduced integration elements do better as they do not cause shear or membrane

locking. This enables the shell elements to achieve deformation to high values of χ. Within plane strain elements, the analysis with CPE8R formulation (simulation L) is seen to give results within 10% of accurate moment calculation. Increased discretization decreases the total error in calculation. Typically, shell elements do not include the calculation of radial stresses. As the radial stresses become significant with the increase in curvature, their effect is seen magnified in the deviation of moment from theory at higher curvatures.

Overall, for MARC, 4-noded plane strain elements are seen to give about -10% error in moment calculation, while 8-noded plane strain elements show an error of about -8%. Equivalent element formulation in ABAQUS shows an error of about -10% and -20% respectively indicating lower springback than predicted by theory.

The decrease in discretization level for the shell elements did not affect the error for the case of work-hardening material but, as reported, the error for perfectly plastic material increased to about 37%. Changing the convergence values by 100 times from the default made about 2% change in the bending moment prediction.

The reduced integration element formulation is typically preferred for forming at high curvatures. Use of fully integrated elements causes *shear locking* of elements which typically produces incorrect results. Reduced integration elements do not show this problem and are preferred over fully integrated elements for such problems. In this study, the reduced integration elements did not prove to be significantly helpful than the fully integrated elements. This can be due to fine meshing of the sheet. Overall the results show 4-node plane strain elements to show smaller deviation from theoretical results than the shell elements. They prove to be better as they include the formulation for including radial stresses as the shell elements typically do not include radial stress in calculations.

TABLE 2

VARIOUS COMBINATIONS OF PARAMETERS UNDER WHICH SIMULATIONS HAVE BEEN CARRIED OUT IN ABAQUS USING A ELASTIC PERFECTLY PLASTIC MATERIAL MODEL

INDEX	No. of elements	Thickness (mm)	Final Radius (mm)	Relative Curvature (X)	Element type	Young's Modulus	No. of integration pts	LOADS	Convergence		
									Forming	Springback	Tolerance
A	10 * 100	4	12.85	0.311	CPE4	73 GPa	NA	COUPLE FORCE	FORCE	FORCE	5.00E-03
B	10 * 100	4	12.85	0.311	CPE4R	73 GPa	NA	COUPLE FORCE	FORCE	FORCE	5.00E-03
C	10 * 100	4	13.32	0.300	CPE4	730 Gpa	NA	COUPLE FORCE	FORCE	FORCE	5.00E-03
D	10 * 100	4	31.26	0.128	CPE8R	73 GPa	NA	COUPLE FORCE	FORCE	FORCE	5.00E-03
E	10 * 100	4	31.26	0.128	CPE8	73 GPa	NA	COUPLE FORCE	FORCE	FORCE	5.00E-03
F	1 * 100	4	19.60	0.204	S4	73 GPa	7	MOMENT	FORCE	FORCE	5.00E-03
G	1 * 100	4	19.30	0.207	S4R	73 GPa	7	MOMENT	FORCE	FORCE	5.00E-03
H	1 * 16	4	14.32	0.279	S4R	73 Gpa	7	MOMENT	FORCE	FORCE	5.00E-03
I	1 * 36	4	17.30	0.231	S4R	73 GPa	7	MOMENT	FORCE	FORCE	5.00E-03

TABLE 3

RESULTS FOR SIMULATIONS CARRIED OUT IN ABAQUS USING AN ELASTIC PERFECTLY PLASTIC MATERIAL

Index	At the end of forming					
	r_c Final radius (mm)	Relative Curvature (X)	Bending moment (N-mm) given by		F_m/t Membrane Stress (Mpa)	Error E_1 (%)*
			HILL's model	FEM		
A	12.85	0.311	231	224.72	3.08	-2.72
B	12.85	0.311	231	224.72	3.08	-2.72
C	13.32	0.300	231	226.04	2.83	-2.15
D	31.26	0.128	231	231.05	-10.67	0.02
E	31.26	0.128	231	231.05	-10.62	0.02
F	18.56	0.216	268	241.29		-9.97
G	12.80	0.313	268	240.15		-10.39
H	17.16	0.279	268	368.24		37.40
I	17.32	0.231	268	355.45		32.63

* Error calculated with respect to Hill's model

TABLE 4

VARIOUS COMBINATIONS OF PARAMETERS UNDER WHICH SIMULATIONS HAVE BEEN CARRIED OUT IN ABAQUS USING A WORK-HARDENING MATERIAL

INDEX	No. of elements	Thickness(mm)	Final Radius (mm)	Relative Curvature (χ)	Element type	No. of integration pts	LOADS	Convergence		
								Forming	Springback	Tolerance
J	10 * 100	4	8.25	0.485	CPE4	NA	COUPLE FORCE	FORCE	FORCE	5.00E-03
K	10 * 100	4	6.70	0.597	CPE4	NA	COUPLE FORCE	FORCE	FORCE	1.00E-02
L	10 * 100	4	8.24	0.485	CPE4	NA	COUPLE FORCE	FORCE	FORCE	5.00E-05
M	10 * 100	4	8.25	0.485	CPE8	NA	COUPLE FORCE	FORCE	FORCE	5.00E-03
N	10 * 100	4	7.99	0.500	CPE8	NA	COUPLE FORCE	FORCE	FORCE	1.00E-02
O	10 * 100	4	8.25	0.485	CPE8	NA	COUPLE FORCE	FORCE	FORCE	5.00E-05
P	10 * 100	4	8.41	0.476	CPE4R	NA	COUPLE FORCE	FORCE	FORCE	5.00E-03
Q	20 * 200	4	9.53	0.420	CPE4	NA	COUPLE FORCE	FORCE	FORCE	5.00E-03
R	3 * 100	4	7.43	0.539	S4R	5	COUPLE FORCE	FORCE	FORCE	5.00E-03
S	3 * 100	4	7.13	0.561	S4R	7	COUPLE FORCE	FORCE	FORCE	5.00E-03
T	1 * 16	4	8.87	0.451	S4R	7	MOMENT	FORCE	FORCE	5.00E-03
U	1 * 36	4	8.55	0.468	S4R	7	MOMENT	FORCE	FORCE	5.00E-03
V	3 * 100	4	7.19	0.557	S4R	9	COUPLE FORCE	FORCE	FORCE	5.00E-03
W	3 * 100	4	7.18	0.557	S4R	11	COUPLE FORCE	FORCE	FORCE	5.00E-03
X	3 * 100	4	7.18	0.557	S4R	11	COUPLE FORCE	FORCE	FORCE	1.00E-02
Y	3 * 100	4	7.18	0.557	S4R	11	COUPLE FORCE	FORCE	FORCE	5.00E-05
Z	3 * 100	4	3.02	1.323	S4R	15	COUPLE FORCE	FORCE	FORCE	5.00E-03
AA	3 * 100	4	2.33	1.718	S4R	15	MOMENT	FORCE	FORCE	5.00E-03
AB	3 * 100	4	7.18	0.557	S4	5	COUPLE FORCE	FORCE	FORCE	5.00E-03
AC	3 * 100	4	7.25	0.552	S4	7	COUPLE FORCE	FORCE	FORCE	5.00E-03
AD	3 * 100	4	7.25	0.551	S4	9	COUPLE FORCE	FORCE	FORCE	5.00E-03
AE	3 * 100	4	7.29	0.549	S4	11	COUPLE FORCE	FORCE	FORCE	5.00E-03
AF	3 * 100	4	7.20	0.556	S4	11	COUPLE FORCE	FORCE	FORCE	1.00E-02
AG	3 * 100	4	7.24	0.552	S4	11	COUPLE FORCE	FORCE	FORCE	5.00E-05

TABLE 5

RESULTS FOR SIMULATIONS CARRIED OUT IN ABAQUS USING 2D CONTINUUM ELEMENTS AND A WORK-HARDENING MATERIAL MODEL

Index	At the end of forming							At the end of springback							
	r_c Final radius (mm)	Relative Curvature (χ)	Bending moment (N-mm) given by			Error E_1 (%)*	F_m/t Membrane Stress (Mpa)	r_c' Final radius (mm)	M_B FEM BM (N-mm)	Error E_2 (%)	F_m/t Membrane Stress (Mpa)	Change in curvature ($\Delta\kappa$)		Error E_3 (%)	Total Error (%)
			DM's model	Crafoord's model	FEM							FEM	Theoretical		
J	8.25	0.485	449.83	452.10	445.48	-1.46	-1.63	8.32	2.10	-0.46	-1.56	9.70E-04	1.06E-03	-8.16	-10.09
K	6.70	0.597	473.11	474.84	470.07	-1.00	-1.45	6.75	1.30	-0.27	-1.55	9.96E-04	1.12E-03	-10.7	-12.06
L	8.24	0.485	449.83	452.10	442.02	-2.23	-1.63	8.31	2.10	-0.47	-1.57	9.70E-04	1.06E-03	-8.17	-10.87
M	8.25	0.485	449.83	452.10	426.66	-5.63	-12.90	8.32	38.41	-8.50	-0.89	9.80E-04	1.06E-03	-7.18	-21.31
N	7.99	0.500	453.26	455.51	440.18	-3.37	-14.53	8.06	39.72	-8.72	-3.67	9.84E-04	1.07E-03	-7.63	-19.72
O	8.25	0.485	449.83	452.10	426.66	-5.63	-12.90	8.32	38.41	-8.50	-0.89	9.80E-04	1.06E-03	-7.18	-21.31
P	8.34	0.480	448.67	450.93	436.2	-3.28	1.06	8.41	1.04	-0.23	-0.65	9.75E-04	1.05E-03	-7.42	-10.93
Q	9.53	0.420	433.84	435.91	429.3	-1.51	-0.42	9.61	0.60	-0.14	-0.42	9.46E-04	1.02E-03	-6.90	-8.56

* Error calculated with respect to Crafoord's model

TABLE 6

RESULTS FOR SIMULATIONS CARRIED OUT IN ABAQUS USING 3D SHELL ELEMENTS AND A WORK-HARDENING MATERIAL

Index	At the end of forming						At the end of springback						
	r_c Final radius (mm)	Relative Curvature (χ)	Bending moment (N-mm) given by			Error E_1 (%)*	r_c' Final radius (mm)	M_B FEM BM (N-mm)	Error E_2 (%)	Change in curvature ($\Delta\kappa$)		Error E_3 (%)	Total Error (%)
			DM's model	Crafoord's model	FEM					FEM	Theoretical		
R	7.42	0.539	461.73	463.85	475.89	2.60	7.48	-1.36E-03	2.94E-04	1.07E-03	1.09E-03	-1.27	1.32
S	7.12	0.561	466.21	468.21	470.92	0.58	7.18	3.80E-06	-8.13E-07	1.06E-03	1.10E-03	-3.38	-2.80
T	8.87	0.451	451.70	443.92	440.95	-0.67	8.94	-1.78E-06	4.01E-07	9.79E-04	1.09E-03	-9.92	-10.59
U	8.55	0.468	445.83	448.08	445.34	-0.61	8.62	-1.65E-06	3.68E-07	1.00E-03	1.05E-03	-4.30	-4.91
V	7.18	0.557	465.41	467.44	479.98	2.68	7.24	-9.30E-03	1.99E-03	1.08E-03	1.10E-03	-1.28	1.40
W	7.18	0.557	465.41	467.44	476.37	1.91	7.24	-3.90E-03	8.33E-04	1.07E-03	1.10E-03	-2.04	-0.13
X	7.18	0.557	465.41	467.44	476.37	1.91	7.24	-3.90E-03	8.33E-04	1.07E-03	1.10E-03	-2.04	-0.13
Y	7.18	0.557	465.41	467.44	476.37	1.91	7.24	-3.90E-03	8.33E-04	1.07E-03	1.10E-03	-2.04	-0.13
Z	7.22	0.554	464.81	466.85	502.16	7.56	7.27	-1.56E-03	3.35E-04	1.08E-03	1.14E-03	-5.99	1.58
AA	7.75	0.516	456.81	459.03	477.42	4.01	7.82	-6.67E-03	1.45E-03	1.05E-03	1.07E-03	-1.95	2.06
AB	6.98	0.573	468.57	470.49	484.89	3.06	7.04	-2.02E-06	4.30E-07	1.09E-03	1.10E-03	-0.33	2.73
AC	7.04	0.568	467.69	469.55	472.63	0.66	7.09	-3.61E-06	7.68E-07	1.07E-03	1.09E-03	-2.58	-1.92
AD	7.20	0.555	465.01	467.04	479.62	2.69	7.26	-3.16E-06	6.77E-07	1.08E-03	1.09E-03	-1.12	1.57
AE	7.25	0.552	464.40	466.45	474.94	1.82	7.31	-3.9E-06	8.35E-07	1.07E-03	1.09E-03	-1.95	-0.13
AF	7.14	0.561	466.21	468.02	479.59	2.47	7.19	-3.43E-06	7.32E-07	1.08E-03	1.10E-03	-1.81	0.67
AG	7.03	0.569	467.79	469.74	477.30	1.61	7.08	-3.17E-06	6.75E-07	1.08E-03	1.09E-03	-1.17	0.44

* Error calculated with respect to Crafoord's model

TABLE 7

VARIOUS COMBINATIONS OF PARAMETERS UNDER WHICH SIMULATIONS HAVE BEEN CARRIED OUT IN MARC USING A WORK-HARDENING MATERIAL

Index	No. of elements	Thickness	Final radius	Relative Curvature (χ)	Element type	Number of Integration Points	Assumed strain	Convergence testing		
								Forming	Springback	Tolerance
AH	10 * 100	4	8.97		ELEMENT 11	NA	YES	FORCE	DISPLACEMENT	1.00E-05
AI	10 * 100	4	8.30	0.482	ELEMENT 11	NA	YES	FORCE	DISPLACEMENT	1.00E-06
AJ	10 * 100	4	9.05	0.442	ELEMENT 11	NA	YES	FORCE	DISPLACEMENT	5.00E-04
AK	10 * 100	4	15.30	0.261	ELEMENT 27	NA	YES	FORCE	DISPLACEMENT	5.00E-04
AL	4 * 100	4	5.55	0.721	ELEMENT 75	5	YES	FORCE	DISPLACEMENT	1.00E-05
AM	4 * 100	4	5.57	0.718	ELEMENT 75	7	YES	FORCE	DISPLACEMENT	1.00E-05
AN	4 * 100	4	5.66	0.707	ELEMENT 75	9	YES	FORCE	DISPLACEMENT	1.00E-05
AO	4 * 100	4	5.66	0.707	ELEMENT 75	11	YES	FORCE	DISPLACEMENT	1.00E-05
AP	4 * 100	4	5.66	0.707	ELEMENT 75	11	YES	FORCE	DISPLACEMENT	1.00E-06
AQ	4 * 100	4	5.60	0.715	ELEMENT 75	11	YES	FORCE	DISPLACEMENT	5.00E-04
AR	4 * 100	4	5.64	0.709	ELEMENT 75	15	YES	FORCE	DISPLACEMENT	1.00E-05

TABLE 8

RESULTS FOR WORK-HARDENING MATERIAL MODEL SIMULATIONS –
2D ELEMENTS (MARC)

Index	At the end of forming							At the end of springback							
	r_c Final radius (mm)	Relative Curvature (X)	Bending moment (N-mm) given by			Error E_1 (%)*	F_m/t Membrane Stress (Mpa)	r_c' Final radius (mm)	M_B FEM BM (N-mm)	Error E_2 (%)	F_m/t Membrane Stress (Mpa)	Change in curvature (Δκ)		Error E_3 (%)	Total Error (%)
			DM's model	Crafoord's model	FEM							FEM	Theoretical		
AH	8.97	0.45	441.45	443.67	431.71	-2.70	-6.56	9.05	4.58	-1.03	-2.40	9.52E-04	1.03E-03	-7.83	-11.56
AI	9.80	0.41	431.21	433.21	421.95	-2.60	-5.85	9.89	0.31	-0.07	-1.89	9.42E-04	1.01E-03	-6.61	-9.28
AJ	9.05	0.44	438.96	441.13	430.66	-2.38	-6.49	9.13	1.00	-0.23	-2.20	9.61E-04	1.03E-03	-6.76	-9.36
AK	15.3	0.26	385.89	385.75	375.75	-2.59	-24.75	15.51	2.18	-0.56	8.73	8.51E-04	8.95E-04	-4.89	-8.04

* Error calculated with respect to Crafoord's model

TABLE 9

RESULTS FOR WORK-HARDENING MATERIAL MODEL SIMULATION –
3D ELEMENTS (MARC)

Index	At the end of forming						At the end of springback						
	r_c Final radius (mm)	Relative Curvature (X)	Bending moment (N-mm) given by			Error E_1 (%)*	r_c' Final radius (mm)	M_B FEM BM (N-mm)	Error E_2 (%)	Change in curvature (Δκ)		Error E_3 (%)	Total Error (%)
			DM's model	Crafoord's model	FEM					FEM	Theoretical		
AL	5.55	0.72	495.89	492.92	520.40	5.57	5.57	9.88	-2.00	7.56E-04	1.18E-03	-35.65	-32.08
AM	5.57	0.72	495.89	492.92	508.80	3.22	5.61	10.40	-2.11	1.19E-03	1.17E-03	1.26	2.37
AN	5.66	0.71	494.02	491.70	516.00	4.94	5.70	9.52	-1.94	1.21E-03	1.17E-03	3.59	6.60
AO	5.66	0.71	494.02	491.70	512.00	4.13	5.70	2.44	-0.50	1.35E-03	1.17E-03	15.19	18.82
AP	5.66	0.71	494.02	491.70	572.80	16.49	5.68	5.20	-1.06	7.28E-04	1.17E-03	-37.74	-22.31
AQ	5.60	0.71	494.02	491.70	514.00	4.53	5.63	6.00	-1.22	1.20E-03	1.17E-03	1.93	5.24
AR	5.64	0.71	494.02	491.70	514.40	4.62	5.68	7.20	-1.46	1.17E-03	1.17E-03	0.40	3.56

* Error calculated with respect to Crafoord's model

CHAPTER 5

CONCLUSIONS AND FUTURE WORK

5.1. Conclusions

The use of finite element simulations for designing sheet metal–forming processes has recently become well established. However, accurate prediction of springback, especially for cases involving large curvatures, is still not routinely feasible. A complete theoretical solution is available only for uniform pure bending of perfectly plastic sheets. In this work, a methodology is developed to achieve uniform pure bending by the application of multi point constraints. The total error (E) in springback prediction is partitioned into three components: error in bending moment prediction for the forming stage (E_1), error due to incomplete unloading during the unloading stage (E_2), and error in predicting the change of curvature corresponding to the change in bending moment (E_3).

For perfectly plastic simulations, 2D elements show good correlation for up to a χ of 0.3, while the 3D elements show error E_1 of about 10% at a value of $\chi = 0.2$. Reducing the number of elements along the bend causes the error to increase to 37%.

Using ABAQUS for a work-hardening material model, the 2D elements show error E_1 of about -2%, while E_2 is found to be less than 1%. The 8-noded elements show a E_1 about -6%, while E_2 reaches -10%. Overall, 2D elements show a negative total error indicating less springback than predicted by theory. The 3D shell elements with reduced integration show a total error of about -2% in most cases, while the fully integrated elements show an error of about 2% indicating a nominal over-prediction of springback.

The 4-noded plane strain elements in MARC showed a total error of -12%, indicating lesser springback than that proposed by the theory. For fully integrated shells, the total error

obtained is of the order of 3% for 7 integration points, increasing up to 18% for 11 integration points. Simulation with 11 integration points show an increased error of about 28%. The 3D elements in MARC indicate an error E_1 of less than 6% with different integration points. While the E_2 error was about 2%. The increase in number of integration points for the simulation did not affect E_1 and E_2 much, while E_3 increased with the increase in number of integration points.

Lowering the discretization increases the error in bending moment calculation as is noted from the perfectly plastic simulation. The use of shell elements with finer discretization yields good correlation for $\chi < 0.4$. Shell element formulation handles the shear locking phenomenon efficiently at finer discretization. Tightening the convergence values more than 100 times from the default values cause a small change of about 2% in the results. 2D plane strain elements show a close correlation with theoretical results and can be used for cases involving bending at high curvatures as they include the effect of radial stress in their formulations.

It is recommended that uniform pure bending can be used as a benchmark for identifying the inherent accuracy of results that can be expected when using any particular combination of parameters in a sheet bending analysis.

5.2. Future Work

The following recommendations are made for future work:

i. Repeat the comparative studies with software such as LS-Dyna, ADINA, ABAQUS/Explicit, etc.

ii. Thick shell elements, that include the effect of radial stresses, can be studied.

iii. Use FEA to study stretch-bending and shear-bending.

iv. Extend the applied concept to doubly curved geometries.

v. Estimate the effect of the elastic core on the theoretical bending moment calculation.

REFERENCES

REFERENCES

ABAQUS Documentation 6.4, ABAQUS Inc.

Boogaard, A. H., Meinders, T., Huetink, J., 2003, "Efficient Implicit Finite Element Analysis of Sheet Forming Processes," International Journal for Numerical Methods in Engineering, 56, pp. 1083–1107.

Cao, J., Liu, Z., Liu, W. K., 1999, "Prediction of Springback in Straight Flanging Operation," Symposium on Advances in Sheet Metal Forming, ASME International Mechanical Engineering Congress and Exposition, MED-Vol. 10, pp. 921–928.

Chu, C. –C., 1991, "The Effect of Restraining Force on Springback," International Journal of Solids Structures, 27, No. 8, pp. 1035–1046.

Crafoord, R., 1970, "Plastic Sheet Bending," Ph. D. dissertation, Chalmers Tekniska Högskola, Göteborg.

Dadras, P.,and Majlessi, S. A., 1982, "Plastic Bending of Work Hardening Materials," *Transactions of ASME*, Vol. 104, pp. 224–230.

Delannay, L., Loge, R.E., Chastel, Y., Van Houtte, P., 2003, "Prediction of residual stresses and springback after bending of a textured aluminium plate," *Journal De Physique. IV : JP*, 105, pp. 175-182.

Forcellese, A., Fratini, L., Gabrielli, F., and Micari, F., 1996, "Computer Aided Engineering of the Sheet Bending Process," Journal of Materials Processing Technology, 60, pp. 225–232.

Hill, R., 1950, *The Mathematical Theory of Plasticity*, Oxford University Press, London.

Leu, D., 1997, "A Simplified Approach for Evaluation of Bendability and Springback in Plastic Bending of Anisotropic Sheet Metals," Journal of Materials Processing Technology, 66, pp 9–17.

Ludwik, P., 1904, "Technologische Studie uber Blechbiegung," Verlag des Deutschen Polytechnischen Vereins in Bohmen, Praha.

Maker, B. N., 1998, "User's Guide to Static Springback Simulation using LS-DYNA", Livermore Software Technology Corporation.

Mattiasson, K., Strange, A., Thilderkvist, P., and Samuelsson, A., 1995, *Simulation of Springback in Sheet Metal Forming*, Shen and Dawson, Rotterdam.

Micari, F., Forcellese, A., Fratini, L., Gabrielli, F., and Alberti, N., 1997, "Springback Evaluation in Fully 3-D Sheet Metal Forming Processes," *Annals of CIRP*, Vol. 46, pp. 167–170.

MSC MARC Manual Volume A: Theory and User Information, MSC Software Corporation.

MSC MARC :Manual Volume B: Element Library, MSC Software Corporation

Paulsen, F., and Welo, T., 1996, "Application of Numerical Simulation in the Bending of Aluminum-alloy Profiles," Journal of Materials Processing Technology, 58, pp. 274–285.

Timoshenko, S. P. and Goodier, J. N., 1970, *Theory of Elasticity,* McGraw Hill Book Company, New York

Voce, E., 1948, "The relationship between stress and strain for homogeneous deformations." Journal of Instrumentation and metallurgy, 74, 537-562

Wollter K., 1950, Bildsames Biegen von Blechen um gerade Kanten. Diss. TH Hannover

Xu, W. L., and Ma, C. H., Li, C. H., Feng, W. J., 2004, "Sensitive Factors in Springback Simulation for Sheet Metal Forming," Journal of Materials Processing Technology, 151, pp. 217–222.

Zhou, D., and 1996, "Bending and Springback Analysis using Membrane Elements," *Engineering Systems Design and Analysis*, Vol. 3, pp. 135–142.

APPENDICES

APPENDIX A

CRAFOORD'S PROCEDURE TO CALCULATE η, ρ, AND κ

Crafoord (1970) provides an iterative procedure to differential equations for η, ρ, and M in terms of κ. These parameters as adapted from Crafoord (1970) are as follows:

Relative sheet thickness, $\eta = \frac{t}{t_0}$

Relative curvature, $\kappa = \frac{t}{r_m}$

Dimensionless quantity, $\rho = \frac{r_n}{r_u}$

Using Crafoord's theory, the change in sheet thickness (η) relative to the change in curvature (κ) is given by

$$\frac{d\eta}{d\kappa} = 0.5\left[\left(\frac{1-0.25\kappa}{\eta^2\rho^2} - 1\right)\right]\frac{\eta}{\kappa}$$

The radius of a neutral axis can be calculated using

$$(\gamma - 2\alpha)\ln\rho + \frac{\beta}{2}(\ln\rho)^2 + \frac{\gamma}{\delta}\rho^{\delta} = \frac{\gamma}{\delta}\left[1 - \left(\frac{1+0.5\kappa}{\eta}\right)^{-\delta} + \left(\frac{1-0.5\delta}{\eta}\right)^{\delta}\right] \tag{A.1}$$
$$-\alpha\left[\ln\left(\frac{1-0.5\kappa}{\eta}\right) + \ln\left(\frac{1+0.5\kappa}{\eta}\right)\right] - \frac{\beta}{2}\left[\left(\ln\left(\frac{1-0.5\kappa}{\eta}\right)\right)^2 - \left(\ln\left(\frac{1+0.5\kappa}{\eta}\right)\right)^2\right]$$

Where α, β, γ, and δ are material constants.

Bending moment is calculated according to the equation

$$\frac{M}{t^2}=\left(\frac{1}{\kappa}+0.5\right)^2\left[\frac{\alpha}{4}-\frac{\beta}{8}+\frac{\beta}{4}\ln\left(\frac{1+0.5\kappa}{\eta}\right)+\frac{\gamma}{2\delta-4}\left(\frac{1+0.5\kappa}{\eta}\right)^{-\delta}\right]+$$

$$\left(\frac{1}{\kappa}-0.5\right)^2\left[\frac{\alpha}{4}+\frac{\beta}{8}-\frac{\beta}{4}\ln\left(\frac{1-0.5\kappa}{\eta}\right)-\frac{\gamma}{2\delta+4}\left(\frac{1-0.5\kappa}{\eta}\right)^{\delta}\right]+$$

$$\left(\frac{\eta}{\kappa}\right)^2\left[\frac{\beta}{8}-\frac{\gamma}{4}+\frac{\gamma}{4-2\delta}\right]+\left(\frac{\rho\eta}{\kappa}\right)^2\left[-\frac{\alpha}{2}-\frac{\beta}{8}+\frac{\beta}{4}+\frac{\gamma}{4}\ln\rho+\frac{\gamma}{4+2\delta}\rho^{\delta}\right]$$

The equations are solved in MAPLE. The code is as follows:

```
##This is based on the algorithm by Crafoord
restart;
with(linalg):
##conversion from A,B,C,D to alpha..... for basically plane
strain relations between sigma(phi)-sigma(r)=2/sqrt(3)*sigma(eq)
Convg_tol := 0.00000000000001; delta_kappa := 0.0001;
Amat:=131.6: Bmat:=32.2: Cmat:=73.5: Dmat:=3.75:
alpha:=2*Amat/sqrt(3): beta:=4*Bmat/3: gama:=2*Cmat/sqrt(3):
delta:=2*Dmat/sqrt(3): t0 := 4;
##equation 4.36 from Crafoord's thesis also equation 16 in DM
paper
deqn:=diff(eta(kappa),kappa)= -0.5*(((1-
0.25*kappa^2)/(eta^2*rho^2))-1)*eta/kappa;
##this is eqn 4.49 from Crafoord's thesis - relating rho to
kappa and eta (rho1 to kappatmp and etatmp eqn1:=(gama-
2*alpha)*ln(rho1)+(beta*ln(rho1)^2/2)+(gama/delta*(rho1^delta))=
gama/delta*(1-(((1+0.5*kappatmp)/etatmp)^(-delta))+(((1-
0.5*kappatmp)/etatmp)^delta))-alpha*(ln((1-
0.5*kappatmp)/etatmp)+ln((1+0.5*kappatmp)/etatmp))-
beta/2*((ln((1-0.5*kappatmp)/etatmp)^2)-
ln((1+0.5*kappatmp)/etatmp)^2);
d_eta := -0.5*(((1-0.25*kappa^2)/(eta^2*rho^2))-1)*eta/kappa *
delta_kappa;
kappatmp:=delta_kappa; rhotmp:=1.0;kappa1[0] := 0; kappa1[1] :=
delta_kappa; eta1[0] := 1; eta1[1] := 1;etatmp := 1;
fd := fopen(`c:/radius/intermed.txt`,APPEND, TEXT);
# Assuming that kappa maximum of interest is 1.0 - to decide
number of increments in kappa.  DO this j loop only if tou want
a curve in terms of kappa.  Otherwise can directly jump to any
kappa of interest by setting kappatmp := kappa
for j from 1 to 1/delta_kappa do
for i from 1 to 500 do
```

```
eta1[j] := eta1[j-1] + subs({kappa = kappa1[j],eta = eta1[j],
rho = rhotmp}, d_eta);
#Numer_rk45:=dsolve({subs(rho=rhotemp,deqn),eta(1e-
200)=1},eta(kappa),type=numeric);
#eta1[i]:=op(2,op(2,Numer_rk45(algsubs(temp=kappatmp,temp))));
etatmp := eta1[j];
rho[j]:=fsolve(eqn1,rho1=0.5..1);
if abs(rhotmp-rho[j])< Convg_tol then
rhotmp :=rho[j];
break;
fi;
rhotmp :=rho[j];
od;
kappa1[j]:=kappatmp;
fprintf(fd,`%4.10f %4.10f %4.10f %d %d
\n`,kappa1[j],eta1[j],rho[j],j, i):
rc1[j] := 1/2*eta1[j]/kappa1[j]*t0*sqrt(4+kappa1[j]^2);
#print(kappa1[j],eta1[j],rho[j],rc1[j], j, i):
kappatmp:=kappatmp+delta_kappa;
kappa1[j+1]:=kappatmp;eta1[j+1] := eta1[j];
od:
fclose(fd);
##After the eta, kappa and rho values are obtained, they are
used to calculate the moment and other required parameters
fd1:=fopen(`c:/radius/intermed.txt`,READ,TEXT);
alldata1:=readdata(fd1,3):
fclose(fd1);
convert(alldata1,array):
fd2:=fopen(`c:/radius/final2.txt`,APPEND,TEXT);
for k from 4845 to rowdim(alldata1) do
## setting the values of kappa, eta and rho from the read array
kappav:=alldata1[k,1]; etav:=alldata1[k,2]; rhov:=alldata1[k,3];
ry := etav * t0/kappav * (1+kappav/2);
rc1 := 1/2*etav/kappav*t0*sqrt(4+kappav^2);
ri := etav * t0/kappav * (1-kappav/2);
t := ry - ri;
rc2 := sqrt((ry^2 + ri^2)/2);
rm := (ry+ri)/2;
ro := (ry^2-ri^2)/(2*t0);
rn:=sqrt(ry*ri);
BM[k]:=evalf((1/kappav+0.5)^2*(alpha/4-
beta/8+beta/4*ln(1/etav+0.5*kappav/etav)+((gama/(2*delta-
4))*((1+0.5*kappav)/etav)^(-delta)))+(1/kappav-
0.5)^2*((alpha/4+beta/8-(beta/4*ln(1/etav-0.5*kappav/etav))-
(gama/(2*delta+4))*((1-
0.5*kappav)/etav)^(delta)))+(etav/kappav)^2*(beta/8-
```

```
gama/4+gama/(4-2*delta))+(rhov*etav/kappav)^2*(-alpha/2-
beta/8+gama/4+beta/4*ln(rhov)+((gama/(4+2*delta))*rhov^delta)));
#this is M/t0^2
actBM[k]:=etav^2*BM[k];
fprintf(fd2,`%4.10f %4.10f %4.10f %5.10f %5.10f %5.10f %5.10f
%5.10f %5.10f %5.10f %6.10f
%6.10f\n`,kappav,etav,rhov,ry,rm,ro,rn,ri,rc1,rc2,BM[k],actBM[k]
);
od;
fclose(fd2);
```

APPENDIX B

FEA MODELS

In the initial phase, displacement boundary conditions were given to the sheet. The governing equations for sheet bending are

$$x = \left(\sqrt{\frac{(\rho_f)}{time} + \frac{t_0^{\,2}}{4}} \sin\left(\frac{x_0}{\rho_f} time \right) \right) - x_0 \tag{B.1}$$

$$y = \left(-\sqrt{\frac{\rho_f}{time} + \frac{t_0^2}{4}} \left(1 - \cos\left(\frac{x_0}{\rho_f} time \right) \right) \right) - y_0 \tag{B.2}$$

Compressive stresses were generated because of the enforced constraint.

Later, the same set of displacement boundary conditions were applied to a dummy beam, as shown in Figure B1. The dummy beam was made a little longer than the sheet so that the contact exists even at high curvatures.

Contact was given at the end of the dummy beam and the last 5 nodes on the center fiber of the sheet. For springback, the contact was released. Even these simulations were found to induce a significant amount of compressive stresses.

Crafoord's theory suggested using a long dummy beam of infinite length compared to the sheet to be bent. A small force is applied on the end of the long dummy rod. This gives a negligible shear stress to the sheet while the sheet is bent mostly due to the effect of the moment caused by the force applied to the end of the sheet. The Simulation has limitations in terms of the convergence criteria. Sheet bends only to a χ of about 0.05 before termination.

Subsequently, model employed in this study was developed. Bending is achieved using a couple force at the right end nodes of the sheet. The region of sheet where the loads are applied deforms severely. Rigid elements are used to distribute the force equally. These elements maintained a rigid structure while the forces were transmitted through the street. Figure B3 shows the schematics of the model.

Figure B1. Model with a dummy beam (length of sheet=100 mm; thickness of sheet = 4 mm; length of dummy beam = 110 mm).

Figure B2. Model with a long arm (dummy beam) used for bending (Sheet length= 50 mm, length of dummy beam = 1500 mm.

Figure B3. Model used for current study (Length=50 mm, thickness of sheet=4 mm).

APPENDIX C

RIKS RAMM PROCEDURE

Modified Riks-Ramm analysis is used to provide an automatic stepping load for the analysis. A general description of Riks-Ramm procedure adapted from MARC manuals (2005) and ABAQUS 6.4.1 documentation (2005) is as follows:

a. Riks analysis is a displacement-based stepping procedure.
b. Loading in an increment is based on the calculated length of the displacement vector for that increment.
c. The arc-length (length of the displacement vector) is given by the formula:

$$C = \Delta U^T * \Delta U \quad \text{(C.1)}$$

d. For the analysis, we give an initial value of load – 'α' (as a fractional value of total load applied for that loadcase). This is the starting load for the analysis (i.e., loading for the first cycle of the first increment of the analysis).
e. The displacements are calculated (for the current cycle) using the following equation:

$$\Delta U = K^{-1} (\alpha) (P) \quad \text{(C.2)}$$

f. Using this force, convergence is calculated and the end of that particular increment is attained.
g. The arc-length is incremented (This is decided by the number of recycles required to complete the previous increment).

The analysis runs are based on the initial loading and the load required at the end of the loadcase. Sometimes the arc-lengths can also be negative leading to a negative, force application. A typical loading profile for Riks analysis is shown in Figure C1. It can be seen

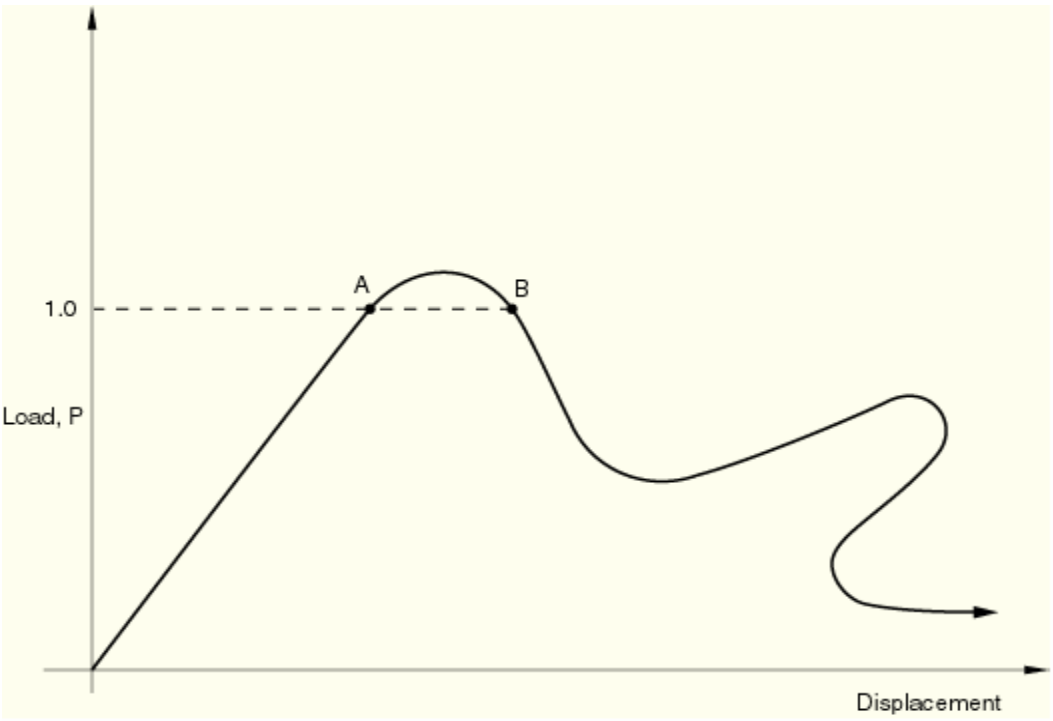

Figure C1. Load applied by FEA software with change in displacement (MARC manuals 2005).

that the load increases and decreases with the arc length. It shows negative arc-lengths with decreasing loads to maintain the equilibrium of the structure.

Also, the loading increments are constrained by the maximum loading allowed in any particular increment or the maximum allowed arc-length in the increment. The loadcase ends when the maximum time (for the loadcase) or the maximum number of increments specified (for the loadcase) is reached.

Typically Riks method is used to solve snap-through problems, where the required force abruptly decreases after the metal snaps. It is also useful for solving ill-conditioned problems such as limit load problems or almost unstable problems that exhibit softening (ABAQUS Analysis Users Manual, 2005).

APPENDIX D

MPC SUBROUTINE

Multi–point constraints (MPC) are given to ensure uniform pure bending of the sheets. When a perfect plastic material model is used for uniform pure bending, the sheet undergoes plastic hinging. This prevents uniform bending of the sheets. The MPC subroutine in ABAQUS provides the capability to enforce multi point constraints. The nodes on the center fiber of the sheet are constrained.

The MPC subroutine is called using *MPC input deck. The following is a detailed description of the subroutine:

```
*mpc, mode=node, user
1,nd508, nd507
2,nd509, nd507
3,nd510, nd507
```

Here, “mode=node” on card I specifies the subroutine where each node is constrained in 2 degrees of freedom (X displacement and Y displacement) simultaneously. First data on card II gives the constraint index, while the second and third data shows the dependant (tied) and independent (free) nodes IDs. Note that the independent node is fixed for all the constraint definitions as the displacement of this node alone controls the geometry of bend.

In the subroutine program, the JDOF parameter is given which activates the specified degree of freedom (X displacement and Y displacement, in this case) for the nodes mentioned in the constraint equation. The “A” matrices provide differential equations based on the nodal constraint equations which help in distributing the loads of the constraint nodes onto the adjacent nodes.

The following is the command line that can be used to run ABAQUS input file with the subroutines:

abaqus job=<filename.inp> oldjob=<restart_filename> user=<subroutine_file.f> cpus=2 double interactive

The user-subroutine is shown below:

```
        SUBROUTINE MPC(UE,A,JDOF,MDOF,N,JTYPE,X,U,UINIT,MAXDOF,
     *LMPC,KSTEP,KINC,TIME,NT,NF,TEMP,FIELD,LTRAN,TRAN)
C
      INCLUDE 'ABA_PARAM.INC'
C
      DIMENSION UE(MDOF),A(MDOF,MDOF,N),JDOF(MDOF,N),X(6,N),
     *U(MAXDOF,N),UINIT(MAXDOF,N),TIME(2),TEMP(NT,N),
     *FIELD(NF,NT,N),LTRAN(N),TRAN(3,3,N)
c  if the initial displacement of Node1 in Y direction is
c  found to be less than or equal to 1e-10, bypass the subroutine
      if (abs(uinit(2,2)) .le. 1.0e-10) then
      LMPC=0
      end if
c  Define X,Y degrees of freedom of Node1 and Node2
      JDOF(1,1)=1
      JDOF(2,1)=2
      JDOF(1,2)=1
      JDOF(2,2)=2
c  Initialize variables to X,Y displacement of Node1, Node2
      xini_tied=X(1,1)
      yini_tied=X(2,1)
      xini_507=X(1,2)
      yini_507=X(2,2)
      dispx_tied=U(1,1)
      dispy_tied=U(2,1)
      dispx_507=U(1,2)
      dispy_507=U(2,2)
c  Obtain the current coordinates of the nodes
      currx_tied=xini_tied+dispx_tied
      curry_tied=yini_tied+dispy_tied
      currx_507=xini_507+dispx_507
      curry_507=yini_507+dispy_507
c  Obtain the theta of nth node and the length of the 1st
c  segment
      thet=atan2(curry_507,currx_507)
      p1=xini_tied/xini_507
      inodepos=anint(p1)
      aleng=sqrt(currx_507**2+curry_507**2)
c  initialize the A matrices
      A(1,1,1)=1
```

```
      A(1,2,1)=0
      A(2,1,1)=0
      A(2,2,1)=1
c initialize eqn_sin=0, eqn_cos=0, eqn_sin1=0 and eqn_cos1=0
      eqn_sin=0
      eqn_cos=0
      eqn_sin1=0
      eqn_cos1=0
      do while (i1 .le. inodepos)
      eqn_sin=eqn_sin+sin((2*i1-1)*thet)
      eqn_cos=eqn_cos+cos((2*i1-1)*thet)
      eqn_sin1=eqn_sin1+(sin((2*i1-1)*thet)*(2*i1-1))
      eqn_cos1=eqn_cos1+(cos((2*i1-1)*thet)*(2*i1-1))
      i1=i1+1
      end do
c
c A(1,1,2) equation
c
      A(1,1,2)=-((aleng*eqn_sin1*(curry_507/currx_507**2)*
     1(cos(thet))**2)+(eqn_cos*curry_507/aleng))
c
c A(1,2,2) equation
c
      A(1,2,2)=-((aleng*(-eqn_sin1)*(cos(thet))**2/currx_507)+
     2(eqn_cos*curry_507/aleng))
c
c A(2,1,2) equation
c
      A(2,1,2)=-((aleng*eqn_cos1*(-curry_507/currx_507**2)*
     3(cos(thet))**2)+(eqn_sin*currx_507/aleng))
c
c A(2,2,2) equation
c
      A(2,2,2)=-((aleng*eqn_cos1*(cos(thet))**2/currx_507)+
     4(eqn_sin*curry_507/aleng))
      RETURN
   END
```

APPENDIX E

TIMOSHENKO-GOODIER THEORY

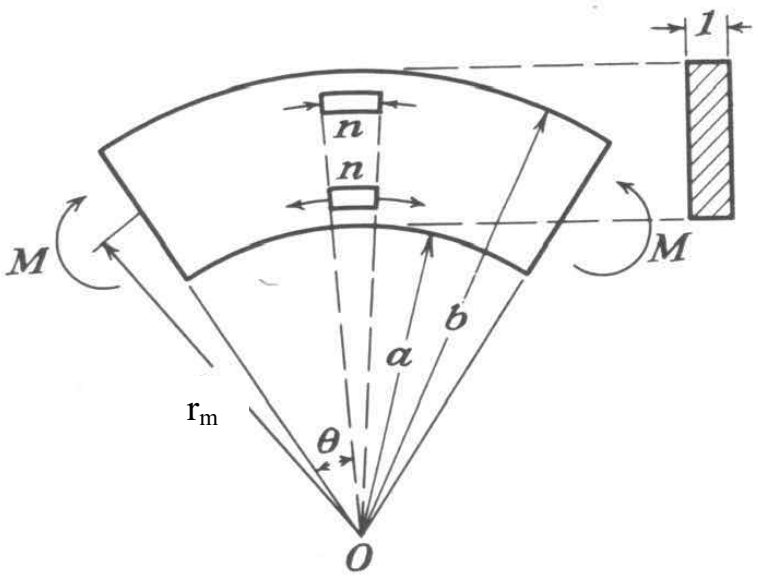

Figure E1. Parameters used in elastic bending theory. (Timoshenko and Goodier, 1951)

Timoshenko and Goodier (1951) proposed the following equations for calculation of radial and circumferential displacements (u and v) of a curved beam subjected to a bending moment M, as shown in Figure E1.

$$u = \frac{1}{E'}\left[-\frac{(1+\nu')A}{r} + 2(1-\nu')Br\log r - B(1+\nu')r + 2C(1-\nu')r\right] + K\cos\theta$$

$$v = \frac{4Br\theta}{E'} - K\sin\theta$$

Where

$$A = -\frac{4M}{N}a^2b^2\log\frac{b}{a}$$

$$B = -\frac{2M}{N}\left(b^2 - a^2\right)$$

$$C = \frac{M}{N}\left[b^2 - a^2 + 2\left(b^2 \log b - a^2 \log a\right)\right]$$

$$N = \left(b^2 - a^2\right)^2 - 4a^2b^2\left(\log\frac{b}{a}\right)^2$$

$$\frac{1}{E'}\left[-\frac{(1+v')A}{r_m} + 2(1-v')Br_m \log r_m - B(1+v')r_m + 2C(1-v')r_m\right] + K = 0$$

Where *u,* the radial displacement and *v,* the circumferential displacement, are given with respect to the polar coordinate system located at the neutral axis (mid-plane) of the curved beam along the symmetry plane. For plane strain, $E' = \frac{E}{1-v^2}$ and $v' = \frac{v}{1-v}$.

The change in curvature can be obtained from the circumferential displacement of any point at angle θ and radius r_{fiber} by the following equations:

$$v = \frac{4Br_{fiber}\theta}{E'} - K\sin\theta$$

$$d\theta = \frac{v}{r_{fiber}} = \frac{4B\theta}{E'} - \frac{K\sin\theta}{r_{fiber}}$$

Note: $d\theta = \frac{v}{r_{fiber}}$ is accurate only for $r_{fiber} = r_m$.

$$dr_m = \frac{r_m d\theta}{\theta} = \frac{r_m B}{E'} - \frac{r_m K}{\theta . r_{fib}}\sin\theta$$

$$d\kappa = \frac{1}{r_m + dr_m} - \frac{1}{r_m}$$